NATIONAL ADVISORY COMMITTEE FOR AERONAUTICS

REPORT 1330

EXPERIMENTAL AND PREDICTED LONGITUDINAL AND LATERAL-DIRECTIONAL RESPONSE CHARACTERISTICS OF A LARGE FLEXIBLE 35° SWEPT-WING AIRPLANE AT AN ALTITUDE OF 35,000 FEET

By HENRY A. COLE, Jr., STUART C. BROWN, and EUCLID C. HOLLEMAN

1957

For sale by the Superintendent of Documents, U. S. Government Printing Office, Washington 25, D. C. Yearly subscription, $10; foreign, $11.25; single copy price varies according to size - - - - - - - - - Price 45 cents

REPORT 1330

EXPERIMENTAL AND PREDICTED LONGITUDINAL AND LATERAL-DIRECTIONAL RESPONSE CHARACTERISTICS OF A LARGE FLEXIBLE 35° SWEPT-WING AIRPLANE AT AN ALTITUDE OF 35,000 FEET

By HENRY A. COLE, Jr., STUART C. BROWN and EUCLID C. HOLLEMAN

Ames Aeronautical Laboratory
Moffett Field, Calif.

National Advisory Committee for Aeronautics

Headquarters, 1512 H Street NW., Washington 25, D. C.

Created by Act of Congress approved March 3, 1915, for the supervision and direction of the scientific study of the problems of flight (U. S. Code, title 50, sec. 151). Its membership was increased from 12 to 15 by act approved March 2, 1929, and to 17 by act approved May 25, 1948. The members are appointed by the President and serve as such without compensation.

REPORT 1330

EXPERIMENTAL AND PREDICTED LONGITUDINAL AND LATERAL-DIRECTIONAL RESPONSE CHARACTERISTICS OF A LARGE FLEXIBLE 35° SWEPT-WING AIRPLANE AT AN ALTITUDE OF 35,000 FEET [1]

By Henry A. Cole, Jr., Stuart C. Brown, and Euclid C. Holleman

SUMMARY

Measured and predicted dynamic response characteristics of a large flexible swept-wing airplane to control surface inputs are presented for flight conditions of 0.6 to 0.85 Mach number at an altitude of 35,000 feet. The report is divided into two parts. The first part deals with the response of the airplane to elevator control inputs with principal responses contained in a band of frequencies including the longitudinal short-period mode and several symmetrical structural modes. The second part deals with the response of the airplane to aileron and rudder control inputs with principal responses contained in a band of frequencies including the Dutch roll mode, the rolling mode, and three antisymmetrical structural modes.

The measured dynamic response characteristics, excited by pulse-type control inputs, are presented in frequency-response form for response quantities at the center of gravity, several locations on the wing, and the tail. The low-frequency part of the response (frequencies below natural frequencies of structural modes) is also presented in transfer function form and comparisons are made with transfer functions predicted by equations of motion which include first-order effects of flexibility. Reasonably good agreement is obtained between experiment and theory for frequencies below the natural frequencies of the structural modes where the assumptions of the equations are valid. Effects of flexibility are shown by comparisons of predicted rigid airplane response with the measured and predicted flexible airplane response.

A method for determination of aerodynamic lift and moment of a flexible wing through use of aerodynamic and structural influence coefficients is presented. Also, relationships between transfer function coefficients and stability derivatives are shown, which in some cases allow stability derivatives to be approximated from flight data.

INTRODUCTION

The desire to increase the range and speed of large airplanes led to configurations with wings of high aspect ratio, thin airfoils, and fuselages of high fineness ratio. All of these factors tend to increase the flexibility of the structure, and the associated aeroelastic effects become of greater importance in problems of static and dynamic stability and control. The dynamic effects are especially important when the airplane is equipped with automatic control because structural modes may introduce system instabilities which would not occur in a rigid airplane. The prediction of these aeroelastic effects is important for rational design of the airplane and its control system.

In view of the above problems, the NACA conducted flight tests on a large flexible 35° swept-wing airplane over a wide range of flight conditions. The aims of this program were to document and analyze the airplane response to control surface motions and, through comparisons between measured and predicted response characteristics, to establish simple but adequate methods of prediction for flexible airplanes. In the present report the longitudinal and lateral-directional responses to control surface motions are documented at an altitude of 35,000 feet over a Mach number range of 0.6 to 0.85. Response quantities at a number of locations on the wing and fuselage are shown so that the response of the entire airplane is fairly well defined. Also, a simple method is developed for the prediction of the response for inputs which are primarily influenced by the low-frequency modes, the longitudinal short period, the Dutch roll, and rolling modes.

With regard to measuring and analytical techniques, the frequency response is a convenient way to express the dynamic-response characteristics in a standard manner which is independent of the particular input from the control surface. Transient response to pilot-applied pulse inputs were measured and transformed to frequency response by means of the Fourier integral, a technique described in references 1, 2, 3, and 4. Although these frequency-response data completely define the response characteristics, operational expressions relating the output response to an input disturbance, known as transfer functions, are a more useful form for detailed analysis or for the synthesis of automatic control systems. These transfer functions may be approximated from the frequency response by a curve-fitting procedure such as described in reference 5 or by matching time histories on an electronic analog as described in reference 3. Comparable predicted transfer functions may be derived from the equations of motion including rigid body and structural degrees of freedom.

Simplifications in these transfer functions appeared justified when the response of interest was limited to the band of frequencies below the structural modes. Consequently, theoretical transfer functions were derived from the rigid airplane stability equations with first-order effects of flexi-

[1] Supersedes NACA RM A54H09 by Henry A. Cole, Jr., Stuart C. Brown, and Euclid C. Holleman, 1954, and TN 3874 by Stuart C. Brown and Euclid C. Holleman, 1956.

bility included. Coefficients were calculated for both the rigid and flexible airplane for comparison with coefficients evaluated from flight-test data. Simplified relationships between transfer-function coefficients and aerodynamic derivatives are used in some cases to obtain aerodynamic derivatives for comparison with estimated derivatives.

The data used in this report were obtained from flight tests conducted at the NACA High-Speed Flight Station and the analysis and reduction of data were a cooperative effort of HSFS and Ames Aeronautical Laboratory.

TEST EQUIPMENT

The test airplane was a Boeing B–47A with General Electric J–47–GE–23 turbojets and with wing vortex generators as shown in figure 1. Physical characteristics are listed in table I. The airplane was fitted with a nose boom for measuring airspeed, altitude, angle of attack, and angle of sideslip, and an optigraph for measuring the movements of target lights on the wing and tail (figs. 1 and 2). Left and right aileron, left and right elevator, and rudder deflections were each measured by three NACA resistance-type control-deflection indicators located at root, midsemispan, and tip. The outputs were recorded on Weston 12-channel and Consolidated 18-channel oscillographs. The pitch, roll, and yaw rates at center of gravity and roll and yaw rates at the tail were measured by self-recording, magnetically damped NACA turn meters, the accelerations at center of gravity and tail by NACA air-damped accelerometers, and the accelerations on the wing by Statham linear accelerometers. The instruments were aligned with respect to the body reference line and locations of the pertinent instruments are shown in figure 2.

TEST PROCEDURE

The flight-test conditions covered Mach numbers from 0.6 to 0.85 at an altitude of 35,000 feet. For longitudinal maneuvers the center of gravity varied from 12 to 30 percent of the mean aerodynamic chord and the gross weight from 110,000 to 120,000 pounds (table II). For lateral-directional maneuvers the center of gravity was approximately 21 percent of the mean aerodynamic chord and the gross weight approximately 115,000 pounds.

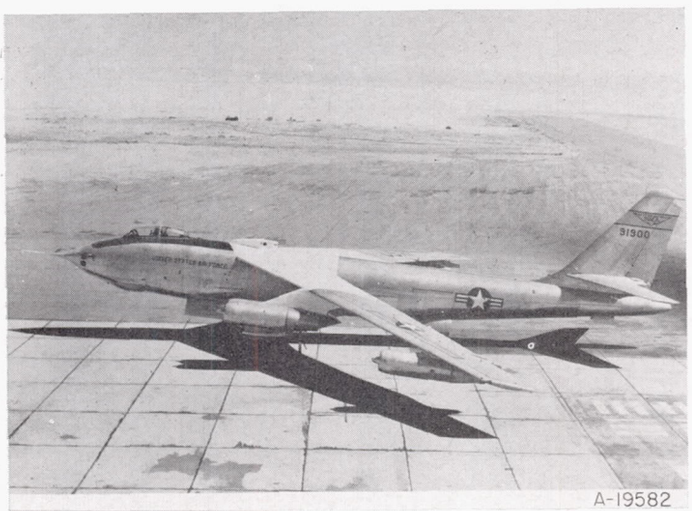

FIGURE 1.—Photograph of the test airplane.

TABLE I.—PHYSICAL CHARACTERISTICS OF THE TEST AIRPLANE

Wing	
Area, sq ft	1, 428
Span, ft	116
Aspect ratio	9. 43
Taper ratio	0. 42
Mean aerodynamic chord, ft	13. 0
Sweepback of quarter-chord line, deg	35
Airfoil thickness ratio (parallel to body center line), percent	12
Dihedral, deg	0
Ailerons	
Area aft of hinge center line (each), sq ft	53. 8
Aileron span to wing span ratio	0. 405
Average aileron chord to wing chord ratio	0. 26
Vertical tail	
Area (including dorsal), sq ft	227
Span, ft	18. 7
Aspect ratio	1. 54
Taper ratio	0. 34
Mean aerodynamic chord, ft	13. 02
Sweepback of quarter-chord line, deg	34. 9
Airfoil thickness ratio (parallel to body center line), percent	10
Distance ¼-chord wing M. A. C. to ¼-chord vertical tail M. A. C., ft	46. 5
Rudder	
Area aft of hinge center line, sq ft	51. 2
Average rudder chord to vertical tail chord ratio	0. 30
Average gross weight-, lb	115, 000
Moment of inertia about the X axis, slug-ft ^{2}	1, 074, 000
Moment of inertia about the Z axis, slug-ft ^{2}	2, 306, 000
Inclination of principal longitudinal axis with respect to fuselage reference line, deg	−2. 6
Horizontal tail	
Area, sq ft	268
Span, ft	33
Aspect ratio	4. 06
Taper ratio	0. 423
Mean aerodynamic chord, ft	8. 57
Sweepback of quarter-chord line, deg	32. 9
Airfoil thickness ratio (parallel to body center line), percent	10
Distance ¼-chord wing M. A. C. to ¼-chord horizontal tail M. A. C., ft	46. 5
Elevator	
Area aft of hinge center line, sq ft	68. 5
Average elevator chord to horizontal tail chord ratio	0. 30

Before each maneuver, the airplane was trimmed at the desired speed and altitude. Then the pilot applied a quick elevator, aileron, or rudder pulse and held controls fixed until the transient motion damped out or, in the case of lightly damped lateral oscillations (yaw damper off), the airplane was allowed to oscillate for about 25 seconds. Typical time histories are shown in figures 3, 4, and 5.

The longitudinal moment of inertia was measured in ground oscillation tests in which the airplane was supported on knife edges and a spring (ref. 6). Other inertia characteristics were estimated.

REDUCTION OF TRANSIENT DATA TO FREQUENCY RESPONSE

The transient data measured in flight represent the dynamic response of the airplane to particular control inputs, whereas for detailed analysis it is desirable to know the airplane response to an arbitrary input. As shown in references 1, 2, and 3, it is possible to transform the input and output response quantities into frequency-response form. This defines the response of the airplane to sinusoidal control-surface motion of various frequencies. Since the response to any arbitrary input may be obtained by applying an inverse transformation to the frequency response, the

TABLE II.—FLIGHT-TEST CONDITIONS

Flight number	Run number	Altitude	Mach no.	C_L	W	c.g.	K_y^2	τ
2	16	36, 170	0. 68	0. 56	121, 400	20. 9	2. 4	5. 8
	18a	35, 500	. 72	. 48	120, 900	20. 9	2. 4	5. 2
	18b	35, 500	. 72	. 48	120, 900	20. 9	2. 4	5. 2
	20	36, 260	. 78	. 41	120, 000	21. 1	2. 4	4. 9
	21	34, 860	. 82	. 38	119, 800	21. 1	2. 4	4. 4
	22	34, 860	. 84	. 33	119, 300	21. 1	2. 4	4. 3
	23	34, 100	. 85	. 28	118, 200	21. 8	2. 4	4. 1
	25	32, 230	. 63	. 49	113, 600	21. 0	2. 5	4. 9
	26	35, 950	. 62	. 61	113, 200	21. 0	2. 5	5. 8
3	15	35, 070	. 63	. 63	116, 100	12. 7	2. 5	5. 6
	16	35, 090	. 66	. 55	115, 900	12. 6	2. 5	5. 3
	17	35, 360	. 71	. 48	115, 900	12. 6	2. 5	5. 0
	18	35, 060	. 74	. 45	115, 900	12. 5	2. 5	4. 7
	19	34, 980	. 77	. 38	115, 900	12. 4	2. 5	4. 5
	20	34, 960	. 81	. 37	115, 700	12. 5	2. 5	4. 4
	21	35, 150	. 82	. 36	115, 600	12. 5	2. 5	4. 3
	22	35, 600	. 84	. 36	115, 500	12. 3	2. 5	4. 3
5	1	35, 840	. 79	. 40	119, 100	24. 9	2. 4	4. 8
	3	34, 170	. 73	. 43	118, 200	24. 8	2. 4	4. 6
	4	34, 070	. 69	. 48	117, 800	24. 6	2. 4	4. 9
	5	34, 220	. 65	. 54	117, 000	24. 6	2. 4	5. 3
	6	35, 100	. 60	. 66	116, 600	24. 6	2. 4	5. 9
	15	35, 950	. 72	. 45	111, 100	21. 6	2. 4	4. 9
9	19	34, 860	. 73	. 43	116, 200	29. 7	2. 4	4. 8
	22	34, 590	. 60	. 60	115, 300	29. 5	2. 4	5. 8
	20	34, 780	. 70	. 43	116, 200	29. 7	2. 4	5. 0
	16	34, 960	. 81	. 37	116, 800	29. 8	2. 4	4. 4

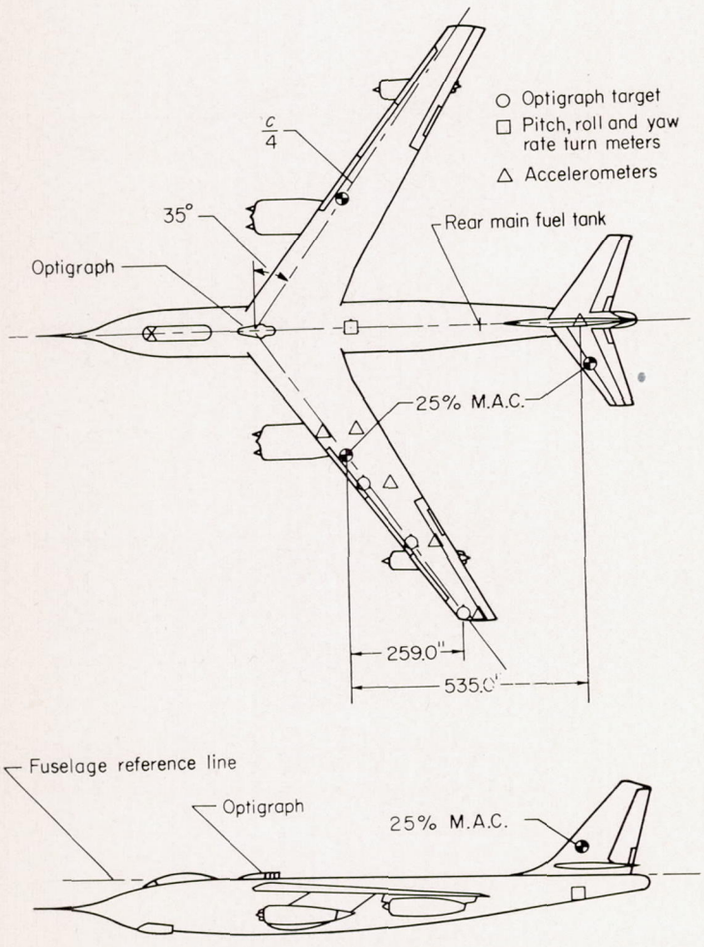

FIGURE 2.—Two-view drawing of test airplane

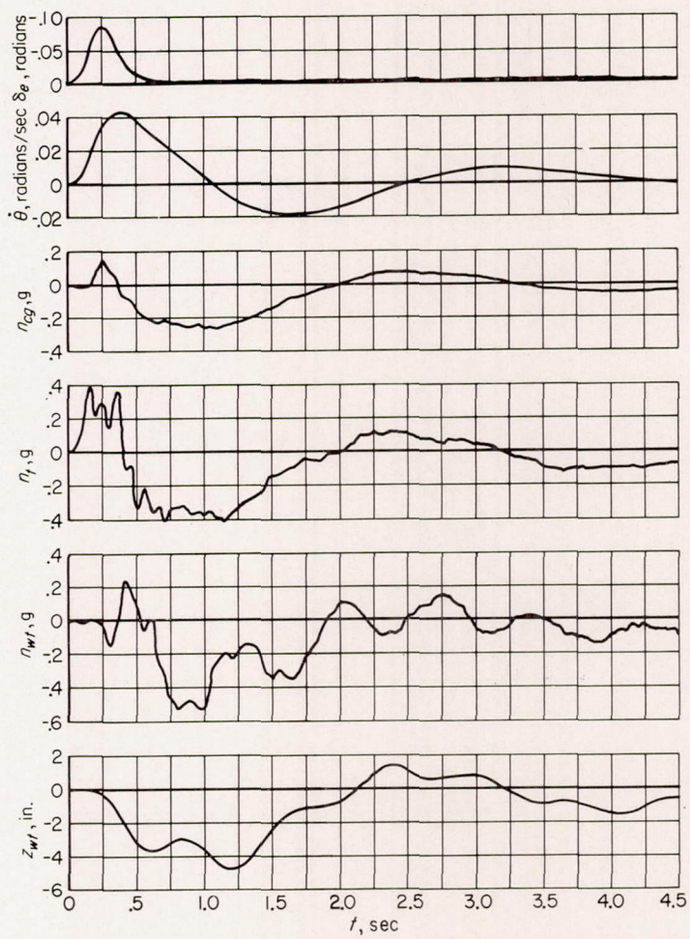

FIGURE 3.—Typical time histories for elevator pulse and response quantities.

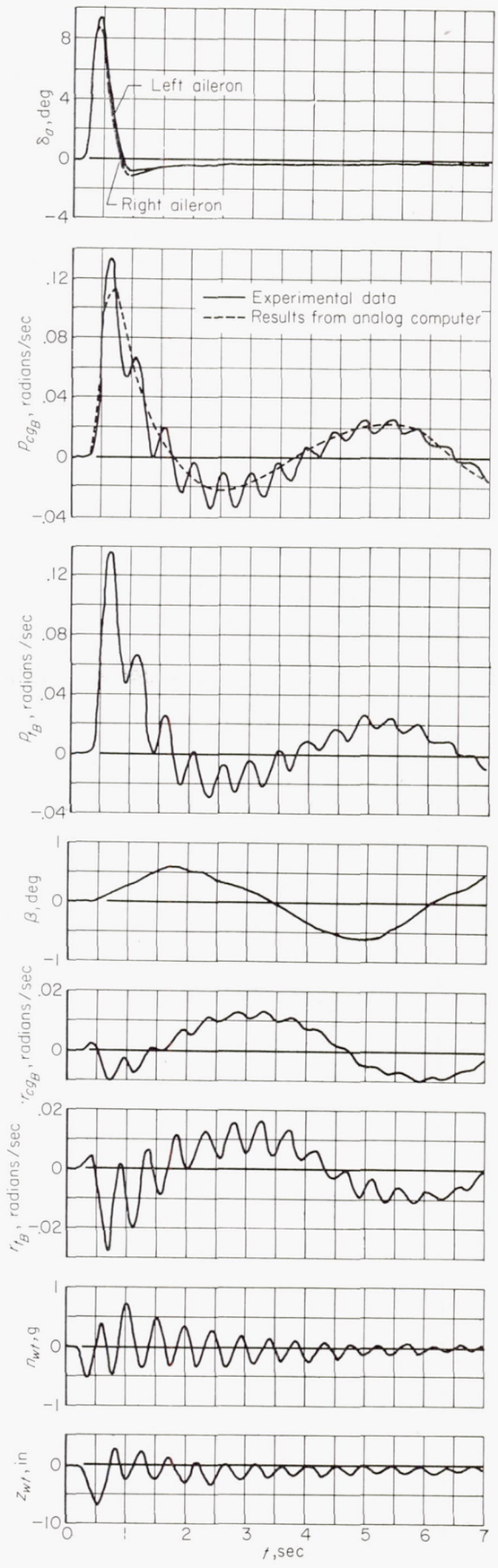

FIGURE 4.—Typical time histories for aileron pulse and response quantities.

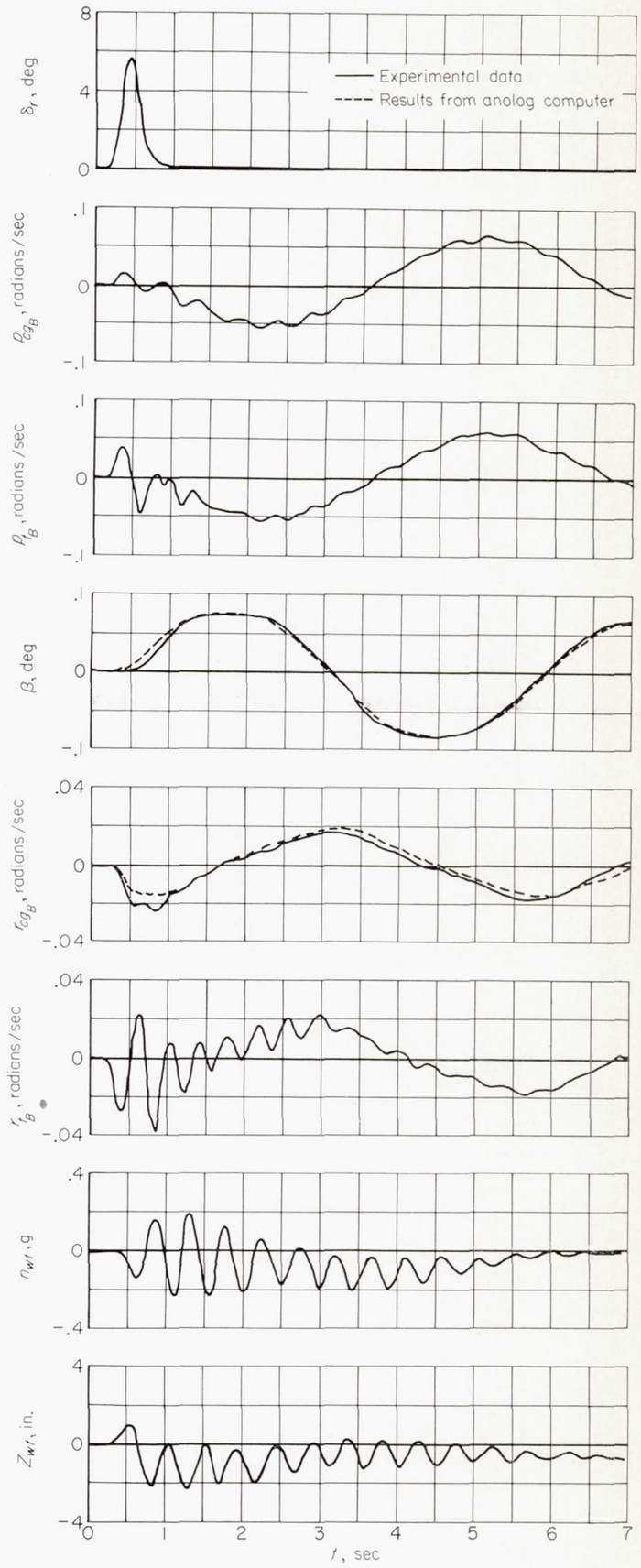

(a) Initial part of time histories.

FIGURE 5.—Typical time histories for rudder pulse and response quantities.

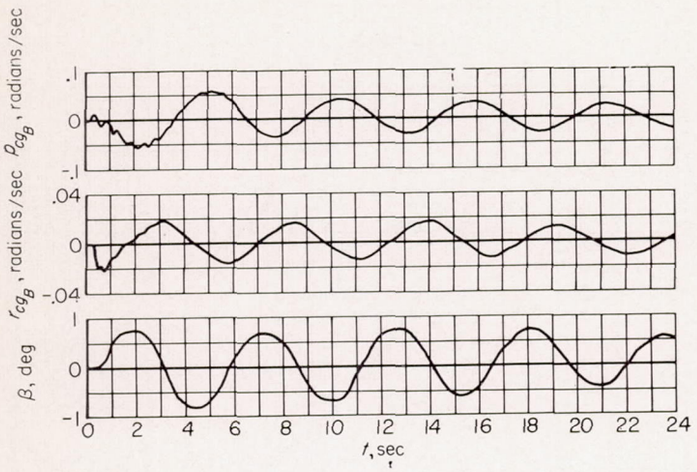

(b) Complete time histories of p_{cg_B}, r_{cg_B}, and β.

FIGURE 5.—Concluded

frequency response defines all of the basic characteristics of the airplane response independently of the particular input, and in itself provides a means for studying the nature of the response and the effect of variables.

METHOD

The Fourier integral was used to convert the transient responses to frequency-response form. The method used for evaluating the Fourier integrals was similar to the one described in reference 7 in which ordinates of the time history are read at uniform intervals such that the time history is closely approximated by a series of parabolic arcs. All traces were read at 0.05-second intervals except for the pitching velocity, wing deflections, and sideslip angle which were read at 0.1-second intervals. The integrals were determined by taking an accumulative sum of the product of the ordinates and the quadrature coefficients for each frequency over the finite length of the record. In cases where the time history did not end on zero, an analytical expression, step or damped sinusoidal oscillation (e. g., ref. 8), was used to evaluate the integral from finite time to infinity. These calculations were performed on a card-programmed IBM 650 digital computer. Corrections were made in the data for the dynamic response of the instruments.

ACCURACY

The accuracy with which the frequency response may be determined is dependent on the relative magnitudes of the transform of the transient quantities and the transform of errors arising from instrument and reading inaccuracies. These errors in the time history were estimated to be of the order of 0.005 inch of film deflection. Therefore, for linear calibration curves, the transform of the errors consists of the Fourier transform of random errors up to about 0.005 inch over the length of the transient plus a step error of 0.005 inch in the analytical correction at the end of the record. The random error was evaluated for a number of traces and was found to be generally smaller than the error in the end correction. For practical purposes the error in the end correction may be considered to be a measure of the maximum expected error. The data in this report were considered to be sufficiently accurate if the amplitude of the Fourier transform of a step of 0.005 inch of film deflection were less than 10 percent of the amplitude of total transform. If the transform of the errors is out of phase with the transform of the transient, then the error in the amplitude will be less than the value above and the phase angle will be in error. However, this phase-angle error will be less than 6° if the amplitude of the error is less than 10 percent of that of the transient. For this reason, accuracy in the amplitude also insures accuracy in the phase angles.

In initial flight tests a number of pilot-applied elevator pulses of varying length were recorded and the amplitudes of their transforms were compared with the above accuracy criterion as shown in figure 6. The error boundary is the amplitude of the transform of a step of 0.6° elevator deflection (which corresponds to 0.005 inch of film deflection multiplied by 10) and represents a boundary of amplitudes below which errors of greater than 10 percent can be expected. The frequency range was selected to include the first two symmetrical structural modes indicated by ground vibration tests in reference 9, and the natural frequencies of these modes are marked on this figure. It may be seen that the transform of the longer pulse (run A) tends to go to zero near the frequency of the wing first-bending mode and falls below the accuracy boundary at regular intervals thereafter. Hence, the longer pulse does not provide adequate excitation for accurate evaluation of the frequency response at frequencies of the structural modes. The shorter pulse (run B), on the other hand, provides adequate excitation for frequencies from 1 to 20 radians per second which is the range of interest in this report. Hence, pulses with a time base of about 0.5 second, as in run B, were used to obtain the frequency-response data in this report. A similar procedure with aileron and rudder inputs indicated that the primary antisymmetric structural modes could be adequately excited with pulse inputs.

REPEATABILITY

Frequency-response curves evaluated from transient data in which the airplane was excited by pulses of different lengths at the same flight condition are compared in figure 7. Also shown in this figure are boundaries below which errors of greater than 10 percent would be expected. This error boundary represents the value of $\dot{\theta}/\delta_e$ for which the sum of the separate errors of $\dot{\theta}$ and δ_e is equal to 10 percent. It may be seen that the curves agree within 10 percent over the range where the accuracy criterion is satisfied. At frequencies below 1 radian per second, the frequency response obtained by the shorter pulse becomes inaccurate and the curves disagree. Also, at frequencies above 7 radians per second, the frequency response obtained by the longer pulse becomes inaccurate and it may be seen that the values become erratic. Also shown in this figure is a frequency response evaluated from transient data excited by a short pulse on another flight in which conditions were slightly different. This curve agrees well with the other frequency-response curve obtained with a short pulse over the frequency range of 1 to 20 radians per second, except that it is displaced upward at all frequencies. As will be shown later, this difference may be accounted for by the difference in the time parameter τ for the two flights. Thus, the data of

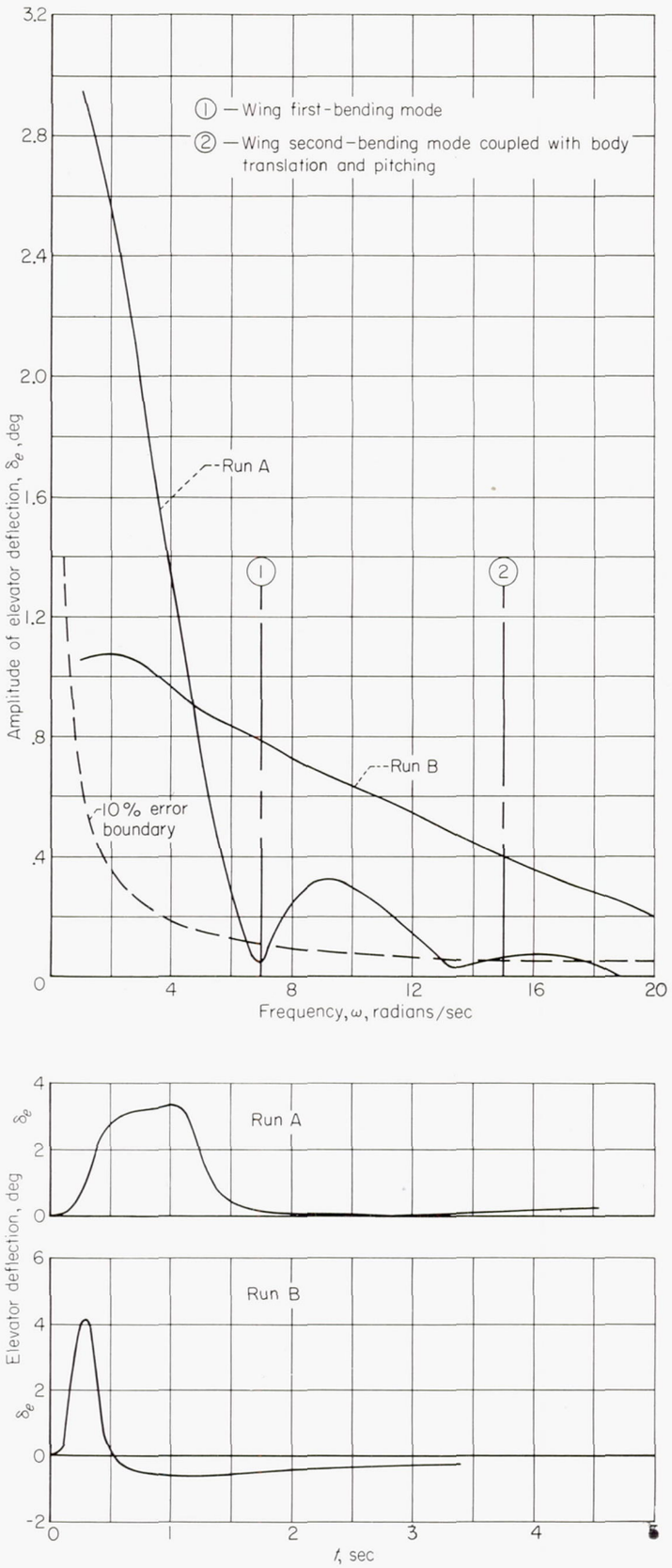

FIGURE 6.—Typical elevator control inputs and the amplitudes of their Fourier Transforms.

figure 7 show that with the short-pulse excitation, the frequency response can be evaluated with sufficient accuracy over the frequency range of interest.

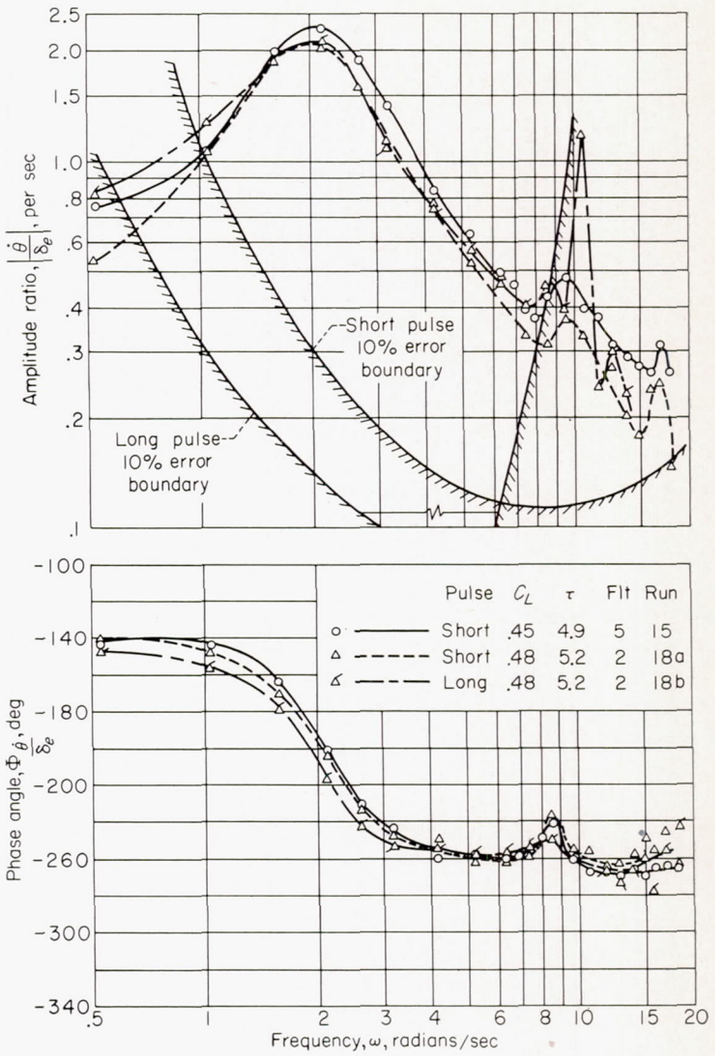

FIGURE 7.—Comparison of pitching-velocity frequency responses obtained from short-pulse and long-pulse imputs; $M=0.72$.

LINEARITY

Since the frequency-response technique is only valid for linear systems, frequency responses are questionable when obtained at flight conditions in which aerodynamic derivatives are believed to be nonlinear. The airplane appears to have a linear response at 0.72 Mach number and 0.48 lift coefficient since the same frequency response was obtained with different degrees of excitation in figure 7. However, a study of wind-tunnel data indicated that for flight conditions above 0.8 Mach number and for lift coefficients above 0.6 at lower Mach numbers the stability derivatives become nonlinear. In view of this factor, caution should be exercised in extrapolating the test results obtained at flight conditions close to these boundaries (see table II for flight conditions) to disturbances greater than those used in the flight tests, that is, $\Delta n_{max}=\frac{1}{4}\ g$ at the center of gravity.

I. LONGITUDINAL RESPONSE CHARACTERISTICS

In the following part of the report, the frequency response to elevator control-surface motions, as determined from the transient flight data, is examined to determine the nature of the flexible airplane response. Then the low-frequency part

of the response is translated into transfer-function form for comparison with values predicted for the rigid and flexible airplane.

MEASURED LONGITUDINAL FREQUENCY RESPONSE

Longitudinal frequency-response curves evaluated by the methods described in Reduction of Transient Data to Frequency Response are shown in figures 8 and 9 for the test range of Mach numbers at an altitude of 35,000 feet; quantities measured at the wing tip and tail as well as at the center of gravity are included so that a fairly complete picture of the response of the airplane is presented. The frequency responses are shown for a forward center-of-gravity location in figure 8 and for a rearward one in figure 9. In the following discussion on these frequency-response curves, the various longitudinal modes will be identified by comparing the accelerations at the center of gravity, wing tip, and tail, and wing deflections. Also, the frequencies at which these modes occur will be compared with those obtained by the ground-vibration tests of reference 9.

SHORT-PERIOD MODE

The first and largest peak in the amplitude ratio of all of the frequency-response curves is the longitudinal short-period mode which occurs at frequencies from 1 to 3 radians per second. These values agree approximately with frequencies estimated from wind-tunnel data. The accelerometer responses at wing tip, tail, and center of gravity, which are compared in figure 10, show that the accelerations at the three locations are essentially in phase, and that the amplitude is about the same as the center of gravity and the wing tip, but is larger at the tail. Differences between accelerations at the various stations are due to contributions of structural deflections and pitching acceleration, which will now be discussed.

The wing-bending deflection response, as determined from optigraph records, is presented in figure 11. At the short-period mode frequency (2 radians/sec), all deflections are similarly phased and increase in amplitude toward the wing tip, representing a type of deflection similar to the wing first-bending mode. Since, for sinusoidal motion, acceleration is equal to minus the frequency squared times the displacement, the contribution of the wing deflection to the amplitude ratio of the acceleration at the wing tip is of the order of $-2.5\ g$ per radian. Optigraph records of tail deflections indicated that the contribution of tail deflection to the amplitude ratio of acceleration at the tail was small at the frequency of the short-period mode.

The contribution of pitching acceleration to the acceleration amplitude at the wing tip and tail may be simply calculated by multiplying the amplitude of the pitching acceleration ($\dot{\theta}\omega$) by the distance to the center of gravity (fig. 2). This is permissible because the phase angles of the acceleration response at the center of gravity and the pitching acceleration response (phase angle of $\ddot{\theta}/\delta$ equals the phase angle of $\dot{\theta}/\delta$ plus 90°) are similar at the frequency of 2 radians per second. The increment in acceleration response at the wing tip and tail, then, is about 2.6 and 5.5 g's per radian, respectively. Hence, at the wing tip the contributions of wing deflection and pitching acceleration tend to cancel each other so that the acceleration amplitudes at center of gravity and wing tip are nearly the same. At the tail, the increase in amplitude is primarily caused by the airplane pitching acceleration.

Comparison of the phase angles in figure 11 with those in figure 10 shows that the wing deflections are in phase with the accelerations and, therefore, the wing tips deflect in proportion to and in the same direction as the airplane accelerates. The following sketch illustrates the relationship of the wing bending to the airplane center-of-gravity-motion. Actually, as shown in the discussion of pitching acceleration, the wing tips travel about the same distance in space as the center of gravity because of the pitching motion of the airplane.

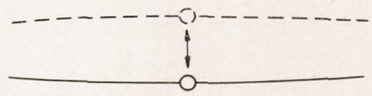

WING FIRST-BENDING MODE

The next peak in the frequency response, as seen in figures 8, 9, 10, and 11, occurs at frequencies of from 8 to 9 radians per second, slightly higher than the wing first-bending frequency (6.9 radians per second) in ground-vibration tests. Calculations indicate that the frequency of this mode is higher in flight than on the ground because of the additional spring force contributed by aerodynamic forces and the increased freedom of the body in pitch and translation. As seen in figures 8 (a) through (c) and 9 (a) through (c), the response peaks for locations on the fuselage are small for this mode as compared to those of the short-period mode, but at the wing tip (figs. 8 (d) and 9 (d)) a very high peak occurs. Referring to figure 10, it is noted that the wing-tip acceleration undergoes a 180° phase shift at this peak. Also, according to figure 11, the amplitudes of the wing deflections increase toward the wing tip and are in phase with each other and 180° out of phase with the wing-tip acceleration which establishes this as the wing first-bending mode. The deflections are also in phase with the acceleration at the center of gravity, as was the case for the short-period mode. The wing first-bending mode is illustrated in the following sketch. The main characteristic which distinguishes this mode from the short-period mode is that the wing deflections are the largest factor in the accelerations at the wing tips, while in the short-period mode the body translation is the largest factor.

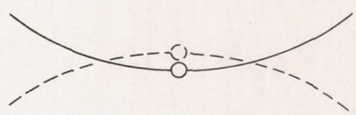

OTHER MODES

Several small peaks appear at frequencies from 14 to 16 radians per second, but these are not well defined because the frequency response is in a region of low accuracy. These peaks are most prominent on the wing-tip acceleration responses (figs. 8 (d) and 9 (d)). The wing-deflection response in figure 11 indicates an upward trend in the midsemispan-deflection amplitude ratio as compared to that of the wing tip. This would indicate a mode of the wing second-bending

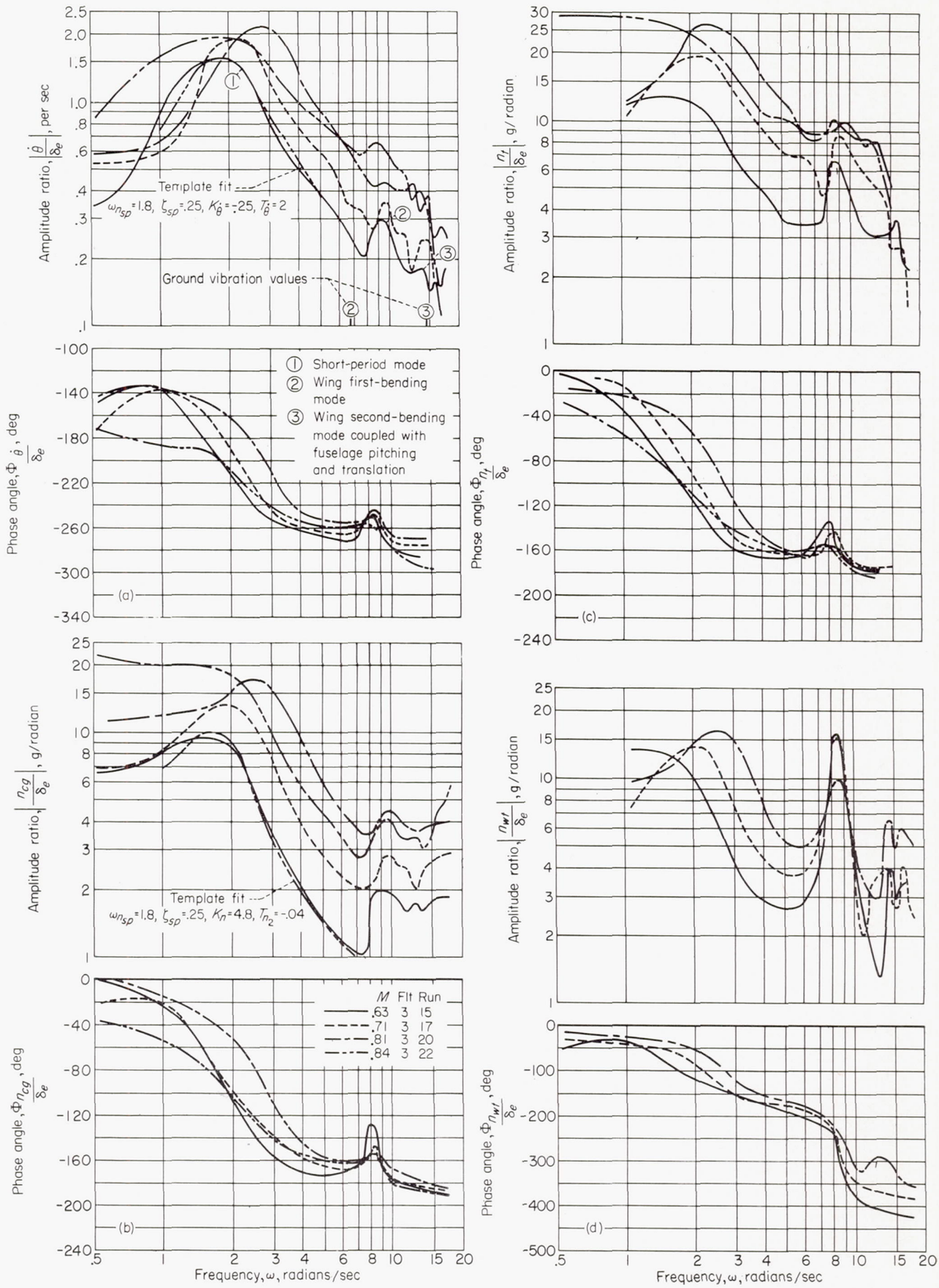

(a) Pitching velocity at the center of gravity.
(b) Acceleration at the center of gravity.
(c) Acceleration at the tail.
(d) Acceleration at the wing tip.

FIGURE 8.—Frequency responses to elevator inputs for the center of gravity at approximately 12.5-percent $\bar{c}$.

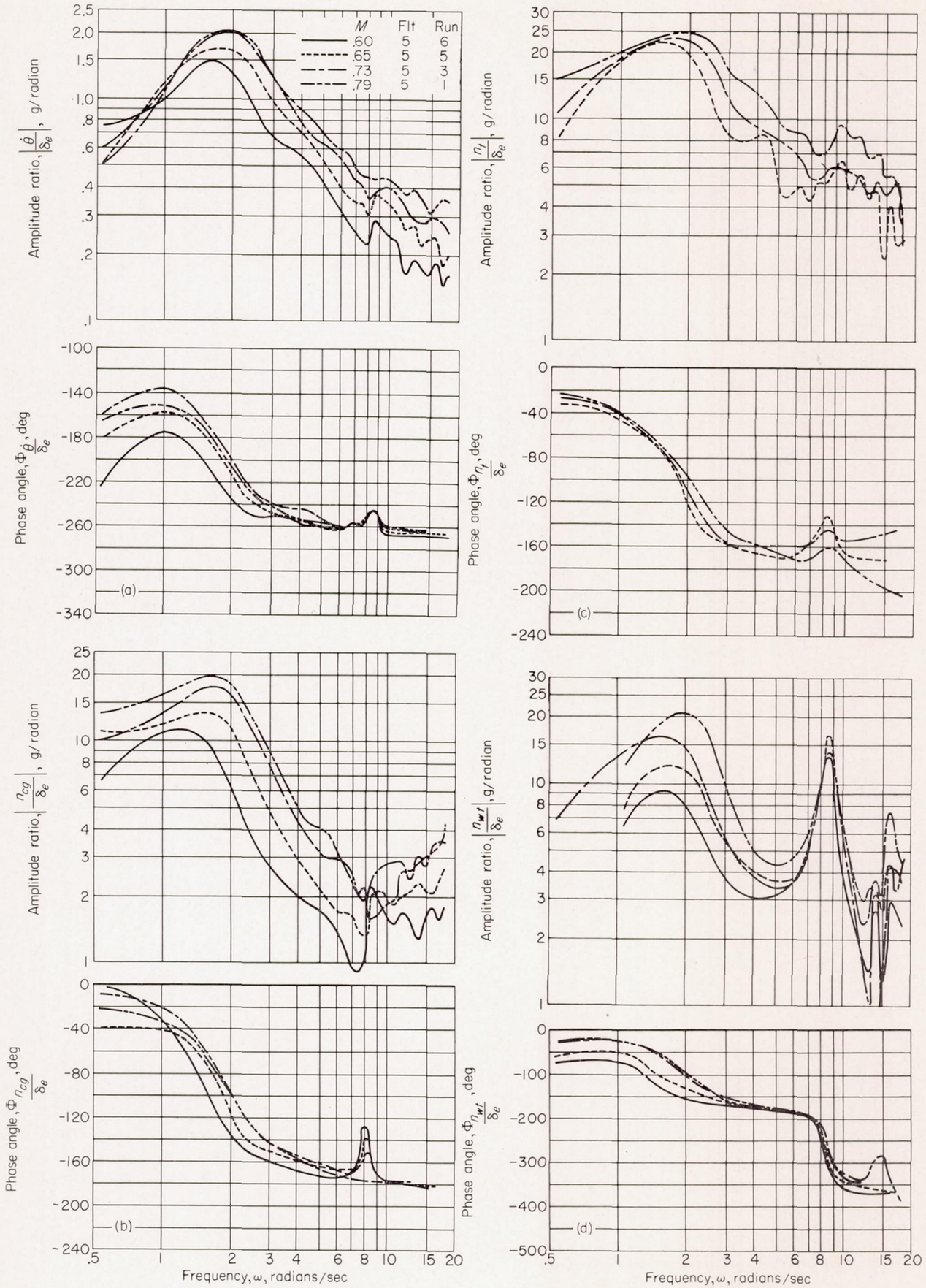

(a) Pitching velocity at the center of gravity.
(b) Acceleration at the center of gravity.
(c) Acceleration at the tail.
(d) Acceleration at the wing tip.

FIGURE 9.—Frequency responses to elevator inputs for the center of gravity at approximately 25-percent $\bar{c}$.

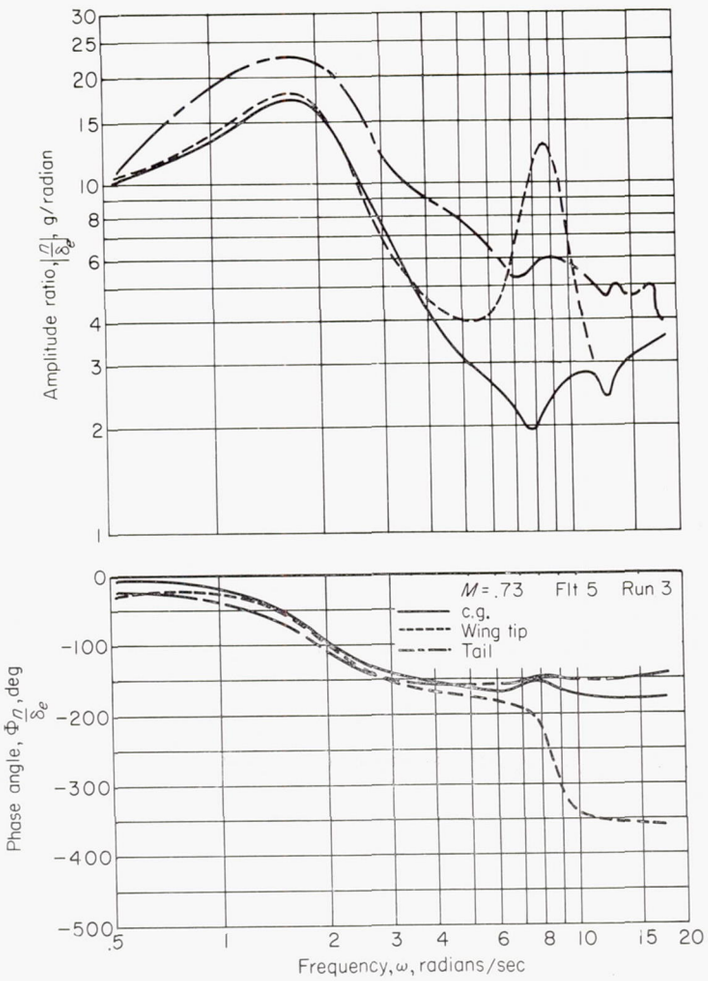

FIGURE 10.—Comparison of acceleration frequency responses to elevator input at several stations on the airplane.

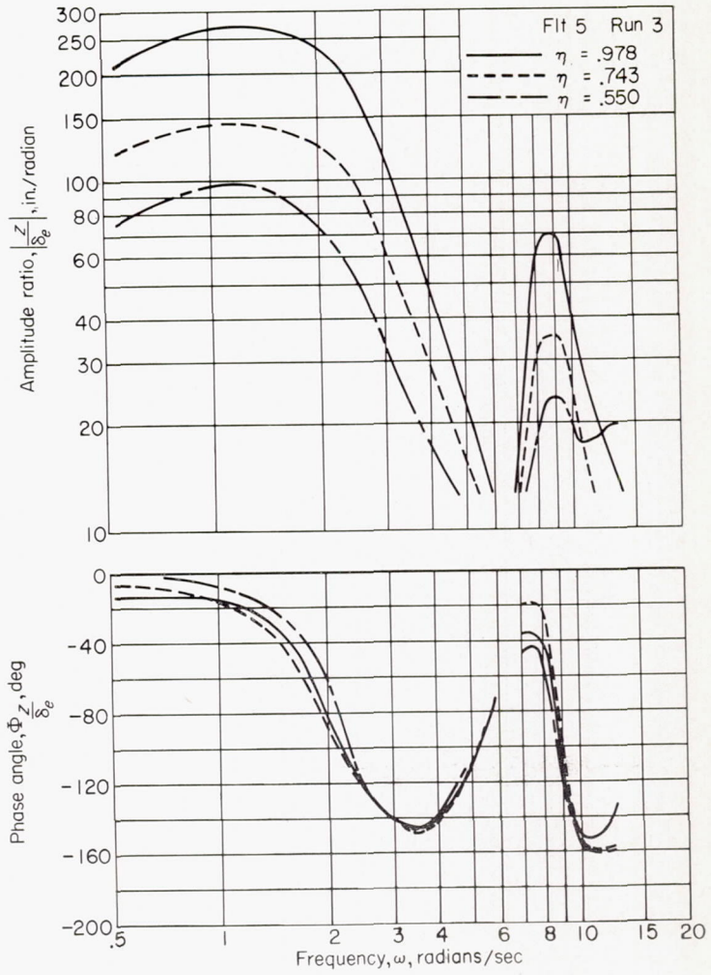

FIGURE 11.—Wing-deflection frequency responses to elevator input for various spanwise stations.

type involving body translation and pitch. Some calculations were made on the modes of vibration of the B–47 with body translation and pitch included; these indicated a mode of the type shown in the following sketch at 16.7 radians per second. This agrees qualitatively with the acceleration frequency responses (figs. 8 (b), (d) and 9 (b), (d)), which show that the accelerations of the wing tip and the center of gravity tend to become more closely phased when the mode becomes prominent at the high Mach numbers. Another possible mode of vibration in this frequency range involves bending of the inboard nacelle supporting structure which, as indicated by ground-vibration tests in reference 9, excites considerable wing motion at 16.4 radians per second. This mode is probably closely coupled with the mode mentioned above, which would explain the appearance of the two closely spaced peaks in this frequency region.

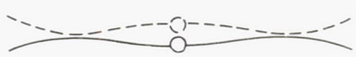

EFFECT OF MACH NUMBER AND DYNAMIC PRESSURE

Since Mach number and dynamic-pressure effects cannot be separated when, as in the present case, data are available for only one altitude, they will be considered together with Mach number arbitrarily selected as the independent variable. From figures 8 and 9 it may be seen that there is a gradual increase in the amplitude of the short-period mode peak for the response quantities up to about a Mach number of 0.81, after which the trend reverses, probably because of critical Mach number effects. The general level of the response quantities also follows this trend at the higher frequencies, although the acceleration at the wing tip seems to be relatively insensitive to Mach number changes. At these higher Mach numbers the frequency response is somewhat dependent on the magnitude of the elevator pulse input because of a nonlinear effect mentioned previously.

The frequency of the amplitude peak of the short-period mode also increases up to a Mach number of 0.81 above which it decreases. The frequencies of the peaks of the higher modes are relatively constant over this range of Mach numbers and dynamic pressures, although the same trend may be noted.

EFFECT OF CENTER-OF-GRAVITY LOCATION

From figure 12 (a) it is seen that the effect of moving the center of gravity from 12.6 to 29.7 has little effect on the frequency response of pitching velocity, although the peaks of the short period mode occur at lower frequencies as the

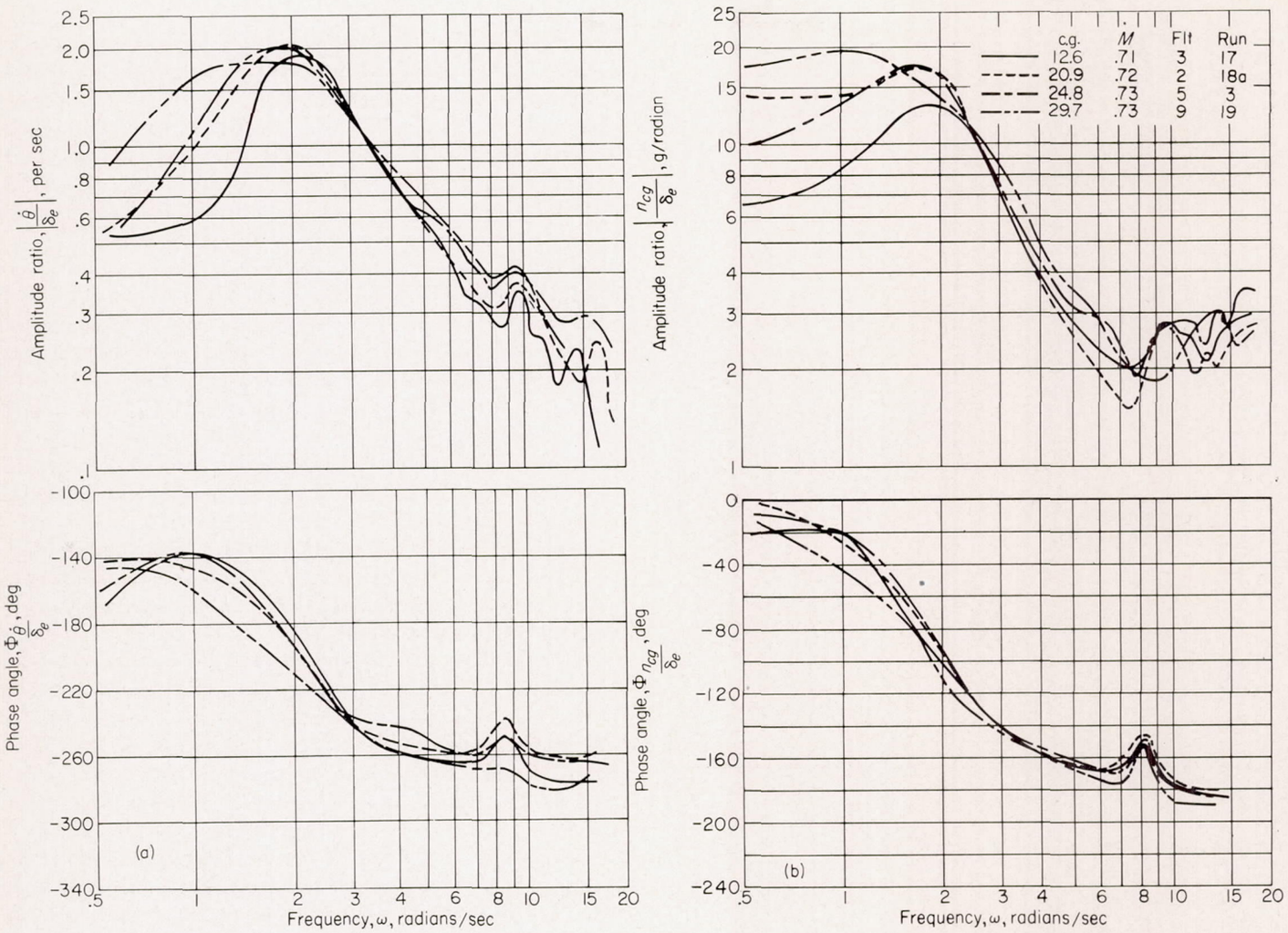

(a) Pitching velocity at the center of gravity.

(b) Acceleration at the center of gravity.

FIGURE 12.—Comparison of frequency responses to elevator inputs for various center-of-gravity locations for approximately the same flight condition.

center of gravity is moved back. The effect of center-of-gravity movement is more apparent on the acceleration response (fig. 12 (b)), which shows a definite trend of the short-period mode to higher peaks and lower frequencies as the center of gravity is moved back.

For the rearward center-of-gravity location there are from 3,000 to 4,000 pounds of additional fuel in the aft main tank (fig. 2) as compared with the forward center-of-gravity location. However, there appears to be no significant change in the high-frequency portion (5 to 15 radians per second) of these responses. This might be expected, since the fuselage vertical-bending mode occurs at a much higher frequency (29 radians per second).

EXPERIMENTAL AND PREDICTED TRANSFER FUNCTIONS

Although frequency-response plots completely defined the response characteristics over the frequency range of interest, analytical expressions for the response are more useful in detailed analyses or in the syntheses of automatic control systems. Such analytical expressions, often called transfer functions, may be evaluated either from the experimental frequency-response plots or from the predicted equations of motion of the airplane. In order to show the relationship between the transfer function and the frequency response more clearly, the predicted transfer functions will be derived first. Then the method for evaluating experimental transfer functions will be explained and, finally, the results of the experimental and prediction methods will be compared.

PREDICTED TRANSFER FUNCTIONS

Equations of motion.—To define completely the airplane dynamic system, the equations of motion must include all of the degrees of freedom, but for practical purposes the degrees of freedom are usually kept to a minimum by including only the most significant airplane modes. In the present analysis, only the short-period mode is considered since it was previously shown that the effects of other modes on the responses of principal interest, those involving motions of the fuselage, were small for the test altitude and range of Mach numbers. However, for response quantities near the wing tip where at frequencies near and above the wing first-bending mode frequency the response is large, these equations are, of course, not adequate.

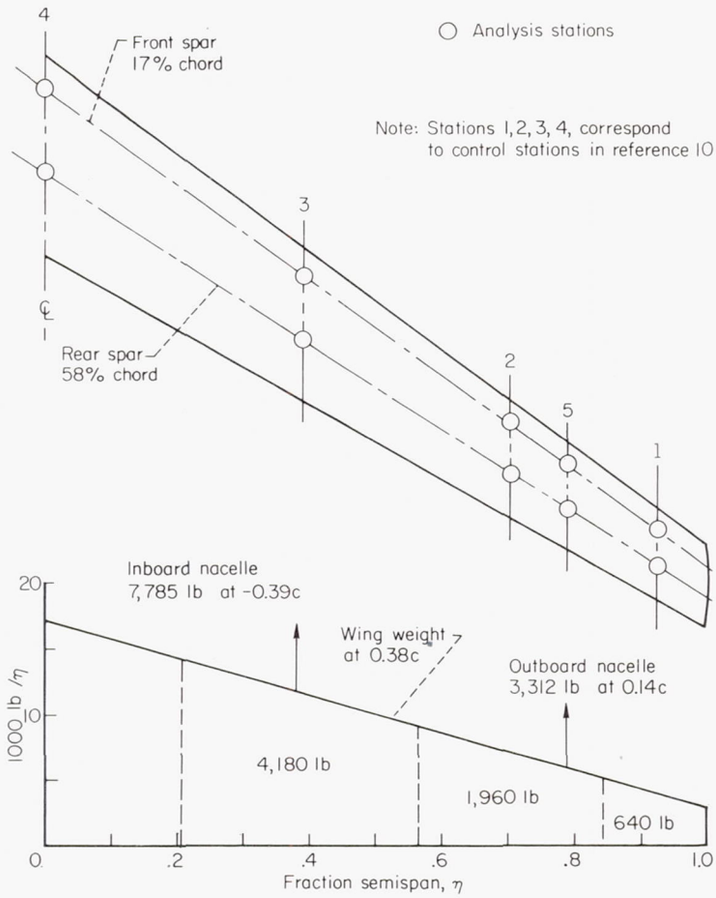

FIGURE 13.—Wing stations and weight distribution used in analysis.

The equations for longitudinal motion, where changes in forward velocity are neglected, were used, with pitching-acceleration ($\ddot{\theta}$) terms added to take account of the distortion of the airplane due to pitching-acceleration inertial loads. These equations in operator form are:

$$[C_{L_\alpha}+(C_{L_{\dot\alpha}}+2\tau)D]\alpha+[(C_{L_{\dot\theta}}-2\tau)D+C_{L_{\ddot\theta}}D^2]\theta+C_{L_{\delta_e}}\delta_e=0 \quad (1)$$

$$(C_{m_\alpha}+C_{m_{\dot\alpha}}D)\alpha+\left[C_{m_{\dot\theta}}D+\left(C_{m_{\ddot\theta}}-\frac{4\tau K_y^2\overline{c}}{2V}\right)D^2\right]\theta+C_{m_{\delta_e}}\delta_e=0 \quad (2)$$

In order to take account of the first-order effects of flexibility in the preceding equations, the structural deformation associated with a coefficient of the variables α or θ and their derivatives was assumed to be in phase with the variable, that is, the damping and inertial forces due to structural motion were neglected.

Estimation of stability derivatives.—Stability derivatives were derived by available theory with the exception of the elevator-effectiveness derivatives, which were modified to include additional Mach number effects indicated by wind-tunnel tests. The general methods applied were those of reference 10 to determine air loads and those of reference 11 to estimate flexibility effects. Mach number effects were included by the Prandtl-Glauert rule as used in reference 10, which was indicated by wind-tunnel tests to be not greatly in error up to a Mach number of 0.75.

In applying the general methods mentioned above, several modifications were made to facilitate use of structural test data. The structural stiffness of the wing was expressed in the form of influence coefficients for the front- and rear-spar chordwise locations which are compatible with the measured influence coefficients and with the spanwise stations used in determining the span loading in reference 10. These wing influence coefficients were obtained from load deflection data presented in reference 12. The weight distribution shown in figure 13 was separated into equivalent weights as indicated and used with the influence coefficients for determining the wing distortion from inertial loadings. Fuselage influence coefficients were obtained from the Boeing Airplane Company, the airplane manufacturer. Table III lists all the influence coefficients, and Appendix B explains how they were used in conjunction with aerodynamic influence coefficients to calculate the lift, moment, and deflection of the flexible wing and tail due to any initial angle-of-attack distribution. The stability derivatives were calculated by determining the initial angle-of-attack distribution due to rigid-body motions or to distortion from inertial loads caused by rigid-body accelerations, and then calculating the resulting lift and moment coefficients by the method in Appendix B. The derivatives and the related factors which were taken into account are summarized in Appendix C.

The values of the calculated derivatives are given in table IV, which lists separately and aerodynamic and inertial contributions. Some of the more important derivatives are compared in figure 14 with values calculated for the rigid airplane. The Mach number effects are reflected by the rigid-airplane derivatives. The flexible-airplane derivatives include both Mach number and flexibility effects and show that flexibility tends to have the opposite effect of Mach number. Of all the derivatives the largest variation occurs in C_{m_α}, but, in general, aeroelastic effects are not exceptionally large because the range of dynamic pressures in these tests is not large.

Evaluation of theoretical transfer functions.—From equation (1) and (2), the following transfer function for pitching velocity may be obtained:

$$\frac{\dot\theta}{\delta_e}=\frac{K_{\dot\theta}(1+T_{\dot\theta}D)}{1+\frac{2\zeta_{SP}}{\omega_{n_{SP}}}D+\frac{1}{\omega_{n_{SP}}{}^2}D^2} \quad (3)$$

and, from the relation $n_{cg}=-\frac{V}{g}(\dot\theta-\dot\alpha)$

$$\frac{n_{cg}}{\delta_e}=\frac{K_n(1+T_{n_1}D+T_{n_2}D^2)}{1+\frac{2\zeta_{SP}}{\omega_{n_{SP}}}D+\frac{1}{\omega_{n_{SP}}{}^2}D^2} \quad (4)$$

The acceleration responses at the wing tip and tail are obtained by adding the contributions of acceleration at the center of gravity, the pitching acceleration, and the structural deflection, so that

$$\frac{n_{wt}}{\delta_e}=\frac{n}{\delta_e}+\frac{x_{wt}}{g}D\left(\frac{\dot\theta}{\delta_e}\right)+\frac{1}{12g}D^2\left(\frac{z_{wt}}{\delta_e}\right) \quad (5)$$

and

$$\frac{n_t}{\delta_e}=\frac{n}{\delta_e}+\frac{x_t}{g}D\left(\frac{\dot{\theta}}{\delta_e}\right)+\frac{1}{12g}D^2\left(\frac{z_t}{\delta_e}\right) \tag{6}$$

where

$$\frac{z}{\delta_e}=\frac{z}{\alpha}\frac{\alpha}{\delta_e}+\frac{z}{n_{cg}}\frac{n_{cg}}{\delta_e}+\frac{z}{\dot{\theta}}\frac{\dot{\theta}}{\delta_e}+\frac{z}{\ddot{\theta}}\frac{\ddot{\theta}}{z} \tag{7}$$

$$\omega_{n_{SP}}=\left[\frac{-C_{L_\alpha}C_{m_{\dot{\theta}}}+C_{m_\alpha}(C_{L_{\dot{\theta}}}-2\tau)}{C_{L_{\ddot{\theta}}}C_{m_{\dot{\alpha}}}+\left(\frac{4\tau K_y^{\,2}\overline{c}}{2V}-C_{m_{\ddot{\theta}}}\right)(C_{L_{\dot{\alpha}}}+2\tau)}\right]^{1/2} \tag{8}$$

$$\zeta_{SP}=\frac{\omega_{n_{SP}}}{2}\left[\frac{-C_{m_{\dot{\theta}}}(C_{L_{\dot{\alpha}}}+2\tau)+C_{L_\alpha}\left(\frac{4\tau K_y^{\,2}\overline{c}}{2V}-C_{m_{\ddot{\theta}}}\right)+C_{m_{\dot{\alpha}}}(C_{L_{\dot{\theta}}}-2\tau)+C_{L_{\ddot{\theta}}}C_{m_\alpha}}{-C_{L_\alpha}C_{m_{\dot{\theta}}}+C_{m_\alpha}(C_{L_{\dot{\theta}}}-2\tau)}\right] \tag{9}$$

$$K_{\dot{\theta}}=\frac{-C_{L_{\delta_e}}C_{m_\alpha}+C_{L_\alpha}C_{m_{\delta_e}}}{-C_{L_\alpha}C_{m_{\dot{\theta}}}+C_{m_\alpha}(C_{L_{\dot{\theta}}}-2\tau)} \tag{10}$$

$$T_{\dot{\theta}}=\frac{-C_{L_{\delta_e}}C_{m_{\dot{\alpha}}}+C_{m_{\delta_e}}(C_{L_{\dot{\alpha}}}+2\tau)}{-C_{L_{\delta_e}}C_{m_\alpha}+C_{L_\alpha}C_{m_{\delta_e}}} \tag{11}$$

$$K_n=-\frac{V}{g}K_{\dot{\theta}} \tag{12}$$

$$T_{n_1}=\frac{-C_{L_{\delta_e}}(C_{m_{\dot{\alpha}}}+C_{m_{\dot{\theta}}})+C_{m_{\delta_e}}(C_{L_{\dot{\alpha}}}+C_{L_{\dot{\theta}}})}{-C_{L_{\delta_e}}C_{m_\alpha}+C_{L_\alpha}C_{m_{\delta_e}}} \tag{13}$$

$$T_{n_2}=\frac{C_{L_{\ddot{\theta}}}C_{m_{\delta_e}}+C_{L_{\delta_e}}\left(\frac{4\tau K_y^{\,2}\overline{c}}{2V}-C_{m_{\ddot{\theta}}}\right)}{-C_{L_{\delta_e}}C_{m_\alpha}+C_{L_\alpha}C_{m_{\delta_e}}} \tag{14}$$

TABLE III.—STRUCTURAL INFLUENCE COEFFICIENTS

(a) Wing

		1,000-pound load at station							
		$3F$[1]	$3R$[1]	$2F$	$2R$	$1F$	$1R$	$5F$	$5R$
Inches deflection at station [1]	3F	0. 0659	0. 0580	0. 1765	0. 1663	0. 2447	0. 2307	0. 2033	0. 1936
	3R	. 0705	. 0931	. 2116	. 2398	. 3057	. 3339	. 2486	. 2784
	2F	. 1769	. 2052	. 7419	. 7795	1. 2134	1. 2490	. 9285	. 9590
	2R	. 1804	. 2318	. 7881	. 9005	1. 3309	1. 4300	. 9995	1. 1070
	1F	. 2302	. 2730	1. 1943	1. 2934	2. 3486	2. 3840	1. 6374	1. 7184
	1R	. 2330	. 2940	1. 2430	1. 4057	2. 4598	2. 5920	1. 7086	1. 8677

(b) Fuselage longitudinal coefficients

Load	Change in stabilizer angle
$1g$ Normal acceleration	−0.45°
1 Radian/sec² pitching acceleration	−0.521° (c.g. = 17 percent), −0.506° (c.g. = 25 percent)
1,000-pound tail load (down)	+0.0342°
1,000 inch-pounds moment applied at stabilizer	0.000207°

(c) Fuselage lateral-directional coefficients

Load	Average change in vertical tail yaw angle due to fuselage and tail flexibility, deg	Change in yaw angle at tail turn meter, deg	Change in roll angle at tail turn meter, deg
1,000 pound aerodynamic load due to sideslip of vertical tail	0. 0685	0. 0342	−0. 0798
1,000 pound aerodynamic load due to rudder deflection	−. 0808	−. 0402	. 0942
$1g$ lateral acceleration	. 581	. 290	----------
1 radian/sec² yawing acceleration	−. 832	−. 415	----------

Note: Wing station locations are shown in figure 13. The letter F denotes front spar location; R denotes rear spar location.

TABLE IV.—PREDICTED LONGITUDINAL STABILITY DERIVATIVES FOR THE FLEXIBLE AIRPLANE AT AN ALTITUDE OF 35,000 FEET; W=100,000 POUNDS

Quantity	c. g.	Mach number				
		0	0. 5	0. 6	0. 7	0. 8
C_{L_α}	------	5. 27	5. 31	5. 36	5. 45	5. 6
Aerodynamic $C_{L_{\dot\alpha}}$	------	7. $1/V$	. 015	. 013	. 011	. 010
Aerodynamic $C_{L_{\dot\theta}}$	0. 12 . 25	$36/V$ 27. $2/V$	. 069 . 050	. 056 . 040	. 046 . 032	. 038 . 025
Inertial $C_{L_{\dot\theta}}$ and $C_{L_{\dot\alpha}}$	. 12 . 25	$.026\frac{V}{g}$ $.027\frac{V}{g}$	. 348 . 373	. 401 . 431	. 444 . 480	. 473 . 512
$C_{L_{\ddot\theta}}$	. 12 . 25	−. 034 −. 030	−. 031 −. 027	−. 030 −. 026	−. 029 −. 025	−. 028 −. 024
C_{m_α}	. 12 . 25	−1. 68 −1. 01	−1. 81 −1. 14	−1. 82 −1. 15	−1. 82 −1. 11	−1. 81 −1. 08
Aerodynamic $C_{m_{\dot\alpha}}$	. 12 . 25	$-27/V$ $-26/V$	−. 053 −. 050	−. 047 −. 045	−. 040 −. 039	−. 036 −. 035
Aerodynamic $C_{m_{\dot\theta}}$	. 12 . 25	$-146/V$ $-138/V$	−. 302 −. 288	−. 256 −. 244	−. 224 −. 213	−. 204 −. 192
Inertial $-C_{m_{\dot\theta}}$ and $C_{m_{\dot\alpha}}$	. 12 . 25	$.024\frac{V}{g}$ $.024\frac{V}{g}$	. 337 . 338	. 398 . 400	. 451 . 457	. 489 . 499
$C_{m_{\ddot\theta}}$	. 12 . 25	. 031 . 030	. 030 . 029	. 029 . 028	. 028 . 027	. 028 . 027
$C_{L_{\delta_e}}$	------	. 327	. 312	. 306	. 299	. 292
$C_{m_{\delta_e}}$	. 12 . 25	−1. 21 −1. 17	−1. 16 −1. 12	−1. 14 −1. 09	−1. 11 −1. 07	−1. 08 −1. 05
τ	------	$2940/V$	6. 05	5. 03	4. 31	3. 77

Since the transfer-function coefficients are complex combinations of the stability derivatives and mass parameters, certain terms have been grouped together so that the coefficients are analogous to the familiar equations for rigid airplanes. The derivatives $C_{L_{\dot\theta}}$ and $C_{L_{\dot\alpha}}$ in the terms $C_{L_{\dot\theta}}-2\tau$ and $C_L+2\tau$ represent primarily the change in effective mass of the airplane resulting from lift due to structural distortions. As seen in table IV, the aerodynamic contributions to these derivatives are relatively small. The derivative $C_{m_{\ddot\theta}}$ in the term $(4\tau K_y^2\overline{c}/2V)-C_{m_{\ddot\theta}}$ represents the change in effective moment of inertia due to pitching moments arising from structural distortions induced by rotational inertial loads.

Using the stability derivatives given in table IV and figure 14 the transfer-function coefficients were calculated for both the flexible and rigid airplane and are shown in figure 15. The coefficient T_{n_1} is not shown because its value is insignificant.

Effect of flexibility on transfer-function coefficients.—The transfer-function coefficients for the rigid and flexible airplane will now be compared to show for the present tests the significance of additional terms included to account for flexibility.

The over-all effect of flexibility on $\omega_{n_{SP}}$ as shown in figure 15 is to reduce the natural frequency by a maximum of about 10 percent. This is principally caused by the reduction in C_{m_α} due to flexibility of the fuselage. This C_{m_α} effect is partially compensated by a significant increase in the $-C_{L_\alpha}C_{m_{\dot\theta}}$ term, which provides an effective spring force resulting from the pitching moments arising principally from wing deflection due to normal acceleration. The term $C_{m_{\ddot\theta}}$ in the denominator tends to increase the frequency by about 5 percent.

The effect of flexibility on damping ratio, ζ_{SP}, is small as shown in figure 15. The damping forces are reduced by flexibility, but the spring and inertial forces are also reduced to such an extent that the over-all effect of flexibility on damping ratio is insignificant.

The pitching-velocity gain, $\frac{\theta}{\dot\theta}$, of the flexible airplane is slightly higher than that of the rigid airplane (fig.15). This change is principally due to the reduction in magnitude of C_{m_α} in the denominator which also is in part compensated by the increase in $C_{m_{\dot\theta}}$. Because of this large contribution of $C_{m_{\dot\theta}}$ for the flexible airplane, increments in gain for a 10-percent increase in τ given in figure 15 show that the

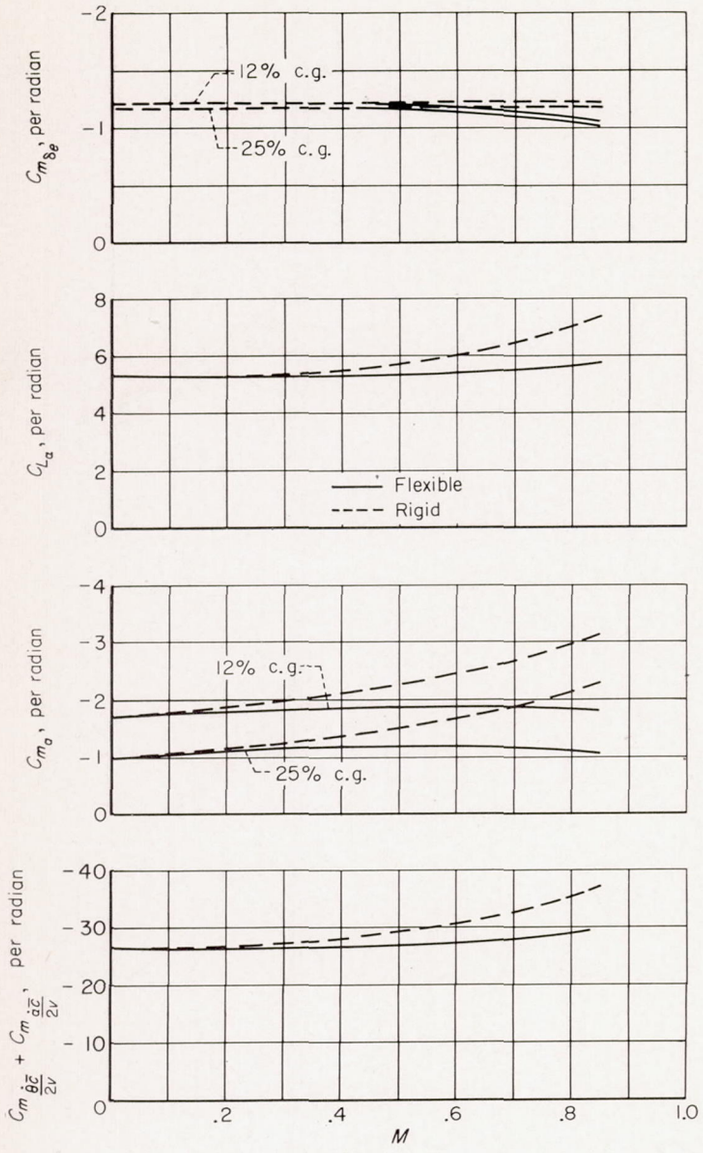

FIGURE 14.—Predicted effect of flexibility on some of the longitudinal stability derivatives at an altitude of 35,000 feet.

flexible airplane has about a 15-percent smaller change in gain due to changes in gross weight and altitude.

Flexibility has little effect on $T_{\dot{\theta}}$ as shown in figure 15. Although the reduction in C_{L_α} due to flexibility tends to increase $T_{\dot{\theta}}$, this is compensated for the most part by the effective reduction in mass in the numerator term.

The discussion of $K_{\dot{\theta}}$ applies to K_n, since these factors are related by a simple constant.

The term T_{n_1} is exceptionally small and is not significant over the range of frequencies considered in this report.

Flexibility tends to increase T_{n_2} (fig. 15). Although this term is small, it does have a noticeable effect at frequencies greater than that of the short-period mode.

Effect of approximate equations on transfer-function coefficients.—Approximate equations are often used for calculating the transfer-function coefficients. These equations, which are obtained by simplifying equations 8, 9, 10, and 11, are as follows:

$$\omega_{n_{SP}}=\left(\frac{-C_{m_\alpha}}{4\tau K_y^2\frac{\bar{c}}{2V}}\right)^{1/2} \tag{15}$$

$$\zeta_{SP}=\left(\frac{-\rho S\bar{c}}{32mKy^2C_{m_\alpha}}\right)^{1/2}\left(2Ky^2C_{L_\alpha}-C_{m_{\frac{\dot{\theta}\bar{c}}{2V}}}-C_{m_{\frac{\dot{\alpha}\bar{c}}{2V}}}\right) \tag{16}$$

$$K_{\dot{\theta}}=\frac{-C_{L_\alpha}C_{m_{\delta_e}}}{2\tau C_{m_\alpha}} \tag{17}$$

$$T_{\dot{\theta}}=\frac{2\tau}{C_{L_\alpha}} \tag{18}$$

Transfer-function coefficients for the rigid and flexible cases were calculated using both the complete and the approximate equations and the results are shown in figure 16.

Coefficients evaluated by the approximate equations show reasonably good agreement with those from the complete equations for the rigid airplane, but large discrepancies are apparent in the case of $\omega_{n_{SP}}$ and $K_{\dot{\theta}}$ for the flexible airplane. This is principally due to the fact that the approximate equations reflect only the large reduction in magnitude of C_{m_α} due to flexibility while in the complete equations, the effect of this reduction in magnitude of C_{m_α} is partially compensated by a substantial increase in the term $-C_{L_\alpha}C_{m_{\dot{\theta}}}$. Hence, it may be seen that $C_{m_{\dot{\theta}}}$ should not be neglected in calculating the frequency and gain of a flexible airplane.

EXPERIMENTAL TRANSFER FUNCTIONS

Experimental transfer functions may be evaluated by applying various curve-fitting procedures to the time histories or to the frequency responses. Curve fitting of a time history may be accomplished by a least-squares fitting method such as described in reference 13. Curve fitting of the frequency response, as in the following analysis, may be done by use of a special set of templates described in reference 5. This method may be explained briefly as follows. It can be shown that an expression for frequency response is obtained by replacing the differential operator, D, in the transfer function by the frequency variable, $i\omega$. The resulting complex number can be factored into first- and second-order terms expressed in polar (amplitude and phase angle) form. The method of reference 5 involves fitting the measured frequency response by graphical addition of templates selected from a set of curves which represent a wide range of first- and second-order factors.

Evaluation of transfer-function coefficients.—As shown previously, the accuracy of the frequency response at low frequencies is questionable. For this reason, template fitting of the frequency response was only considered to be valid for frequencies above 1 radian per second. This limitation made it difficult to fit the frequency response by a unique combination of templates for all of the numerator and denominator terms which are involved simultaneously in the frequency-response expression. Because of this, the natural frequency and damping ratio were determined by a least-squares curve-fitting method (similar to that of ref. 13) of the pitching-velocity time history over the portion of the record in which rate of change of elevator position could

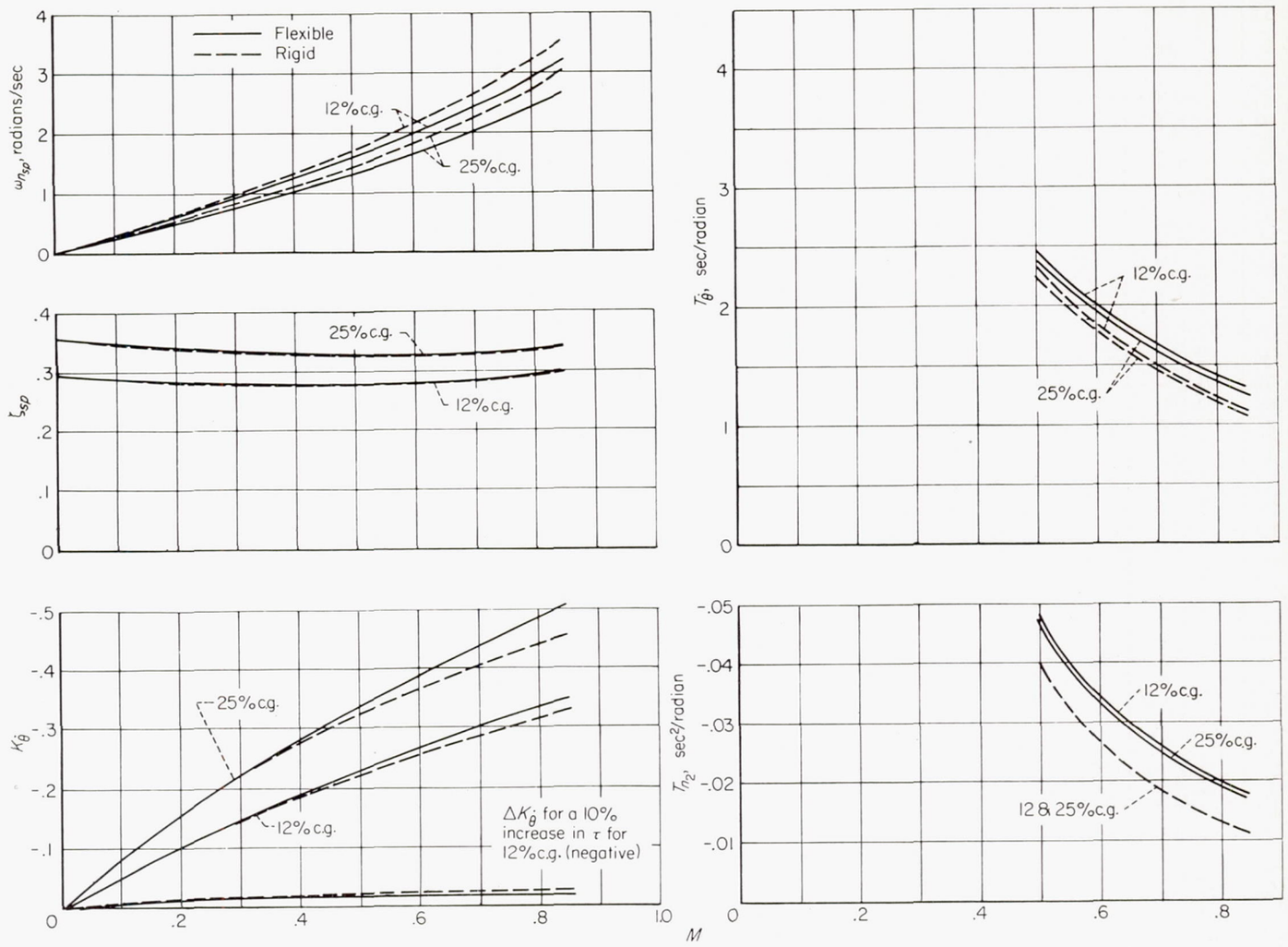

FIGURE 15.—Predicted longitudinal transfer-function coefficients at an altitude of 35,000 feet; $W = 100{,}000$ pounds, $K_y^2 = 2.4$.

be neglected. The appropriate templates for these values of damping ratio and natural frequency were then fitted to the center-of-gravity acceleration frequency-response curves to obtain the acceleration gain, K_n, and the time constant, T_{n_z}. The gain $K_{\dot{\theta}}$ was then determined from K_n. By use of this value of $K_{\dot{\theta}}$ and the previously determined values of ζ_{SP} and $\omega_{n_{SP}}$, the pitching-velocity frequency response was fitted to determine $T_{\dot{\theta}}$. A typical template fit is shown in figures 8(a) and (b) for the 0.63 Mach number curve.

Transfer-function coefficients evaluated from experimental data for the forward and rearward center-of-gravity locations are plotted in figure 17. These values were corrected to a common altitude and gross weight in accordance with predicted variations, but in general these corrections were small.

COMPARISON OF EXPERIMENTAL AND PREDICTED TRANSFER FUNCTIONS

Predicted transfer-function coefficients for the rigid and flexible airplane are also shown in figure 17 for comparison with the experimental values. The moment of inertia used in the predicted coefficients was determined from ground-oscillation tests for the basic airplane (ref. 6), with corrections made for condition of the fuel tanks. The stability derivatives of the table IV were employed.

Effect of Mach number.—Referring to figure 17, it may be seen that the experimental values of natural frequency show good agreement with the predicted values for the flexible airplane and fall about 10 percent below those predicted for the rigid airplane. An exception is noted at a Mach number of 0.84 where the measured frequency decreases sharply, probably due to the large decrease in C_{m_α} as the airplane approaches the pitchup. Also on this figure, it is seen that the scatter in the measured damping-ratio points prohibits definite confirmation of the predicted small variations with Mach number, center-of-gravity location, and flexibility. However, the general level of the values shows good agreement with theory.

In figure 17 good agreement is indicated for the pitching-velocity gain except at Mach numbers of 0.8 and higher, where large unpredicted increases in the measured gain are apparent. This again is probably the result of the sudden decrease in the static margin as the critical Mach number is approached as previously mentioned. On this figure, good agreement also is indicated for the pitching-velocity time constant, $T_{\dot{\theta}}$, although the experimental values tend to fall consistently a small amount below the predicted ones.

Effect of center-of-gravity location.—In figure 18, the variation of natural frequency and damping ratio with center-of-gravity location is shown for several Mach numbers. The measured values of natural frequency show good agreement with the frequencies predicted for the flexible airplane over the test range of center-of-gravity locations. The frequencies predicted for the rigid airplane are consistently higher than those for the flexible airplane, but show about the same variation with center-of-gravity movement as for the flexible airplane. The measured and predicted damping ratios show fairly small changes with center-of-gravity location.

In summary, the longitudinal response of the airplane may be adequately predicted by the theory used herein to take account of flexibility up to a Mach number of 0.8. The largest errors occur in the natural frequency if flexibility is not taken into account, but in general all of the transfer-function coefficients show only small changes over the airplane range of dynamic pressures at 35,000 feet.

Since the transfer-function coefficients are relatively insensitive to flexibility effects at these flight conditions, a more sensitive transfer function, the wing-tip deflection response, was calculated from equation (7) in order to provide a more accurate check on the aeroelastic calculations. The method of calculating deflections is shown in Appendix B. The comparison between experimental and predicted

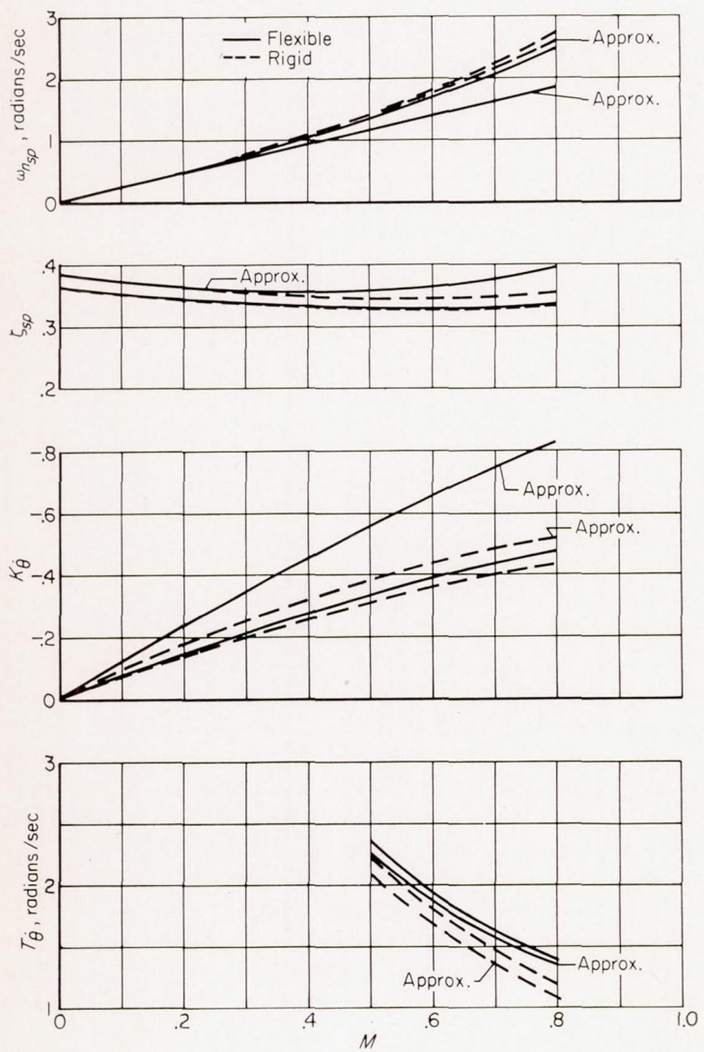

FIGURE 16.—Comparison of longitudinal transfer-function coefficients calculated from the approximate equations with those from the complete equations for the flexible and the rigid airplane; $W = 100{,}000$ pounds, $c.\ g. = 25$-percent M. A. C.

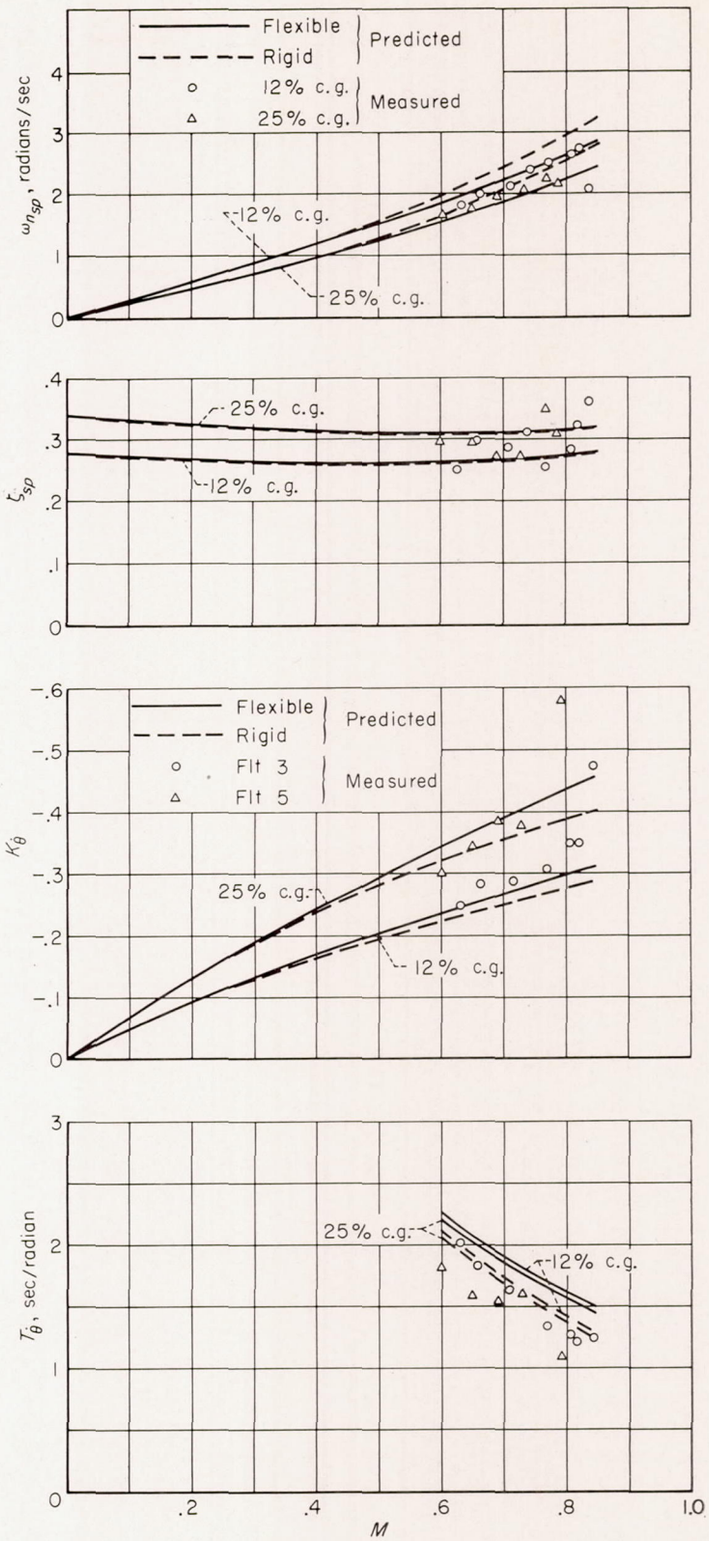

FIGURE 17.—Comparison of predicted and experimental values of longitudinal transfer-function coefficients; $W = 115{,}000$ pounds.

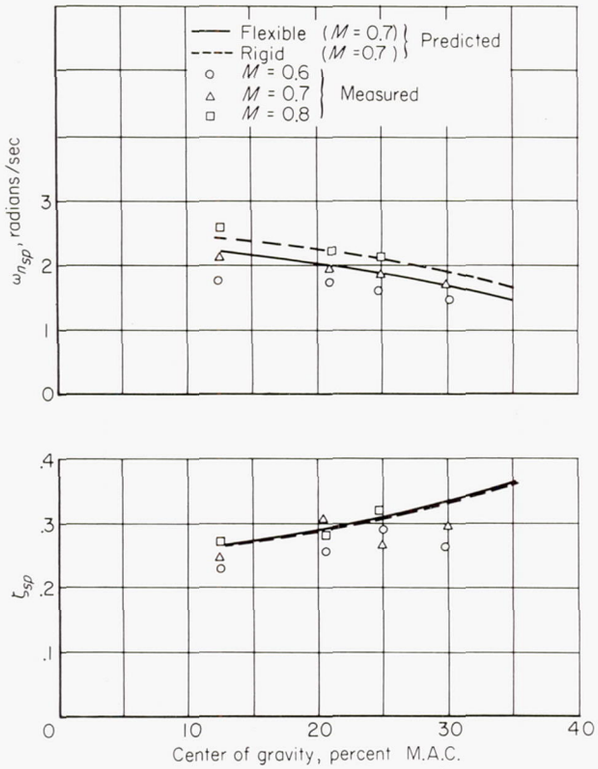

FIGURE 18.—Comparison of predicted and experimental variation with center-of-gravity position of natural frequency and damping ratio of the short-period mode; $W = 115{,}000$ pounds.

values in frequency-response form is shown in figure 19. It may be seen that the amplitude ratios agree very well and that the phase angles of the experimental response tend to lag the predicted ones 20° to 30° up to frequencies of 5 radians per second. From this, it would appear that the theoretical calculations of the contribution of the wing to the stability derivatives are accurate except for a small phase lag which is probably due to the inertial and damping forces due to wing bending motion which were neglected in the theory.

II. LATERAL-DIRECTIONAL RESPONSE CHARACTERISTICS

In the following part of the report, the equations of lateral-directional motion are presented first to give the reader the background needed to interpret dynamic response characteristics in terms of transfer functions and stability derivatives. Frequency responses determined from transient flight data are then examined with this knowledge and comparisons are made between predicted flexible and rigid airplane transfer-function coefficients and those evaluated from flight data. Finally, aerodynamic derivatives extracted from the transfer-function coefficients are compared with estimated derivatives.

PREDICTED RESPONSES

As in the longitudinal case, considerable simplification in the equations of motion can be realized if the structural deformations are assumed to be in phase with the aerodynamic and inertial loads resulting from airplane motions.

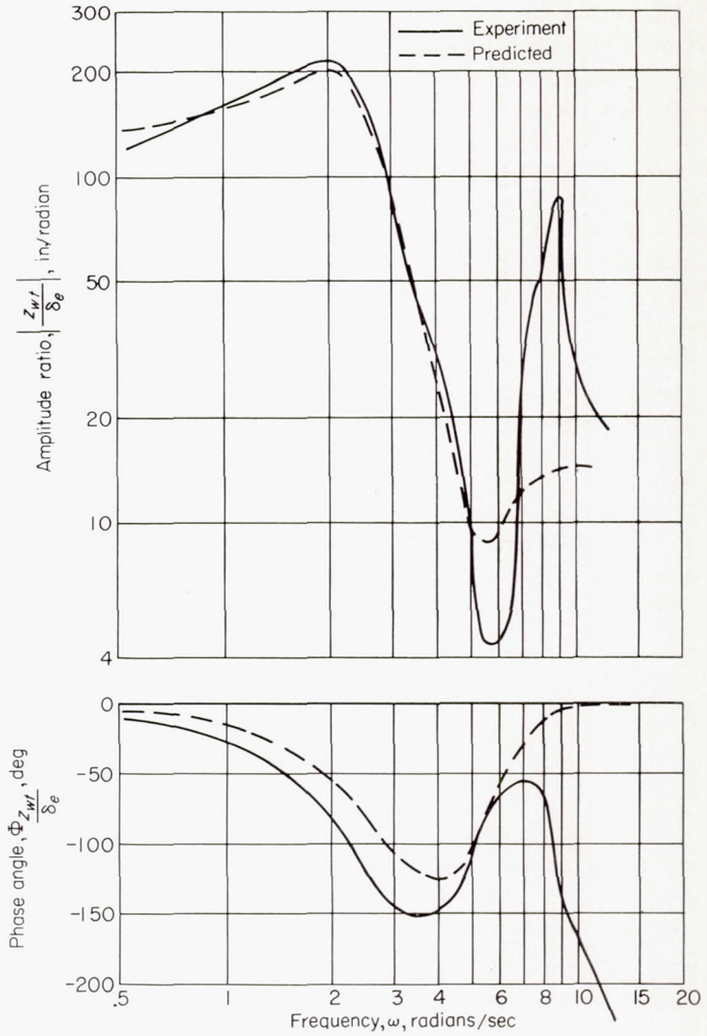

FIGURE 19.—Comparison of experimental and predicted wing-tip-deflection frequency response to elevator input; flight 3, run 17.

The aerodynamic forces arising from these deformations are included by modifying the derivatives in the lateral-directional equations of motion for a rigid airplane.

EQUATIONS OF MOTION

Three-degree-of-freedom lateral-directional equations of motion with respect to stability axes are given in Appendix D. For the flexible airplane appropriate derivatives corresponding to structural deflections due to inertial and deadweight forces resulting from airplane motions have been added to the equations. These additional terms are then combined with the corresponding rigid airplane inertias to form an effective inertia for the flexible airplane. As explained in Appendix D, it was found to be permissible to neglect a number of the inertial derivatives since the cumulative effect of these quantities on the transfer-function coefficients was found to be negligible.

AERODYNAMIC DERIVATIVES

The stability derivatives were obtained by available theory and wind-tunnel data. Effects of structural deflections on the derivatives were obtained through use of aerodynamic and structural influence coefficients in the

manner described in Appendix B. The chordwise centers of pressure of all aerodynamic loads, except loads due to the rudder and ailerons, were assumed to be at the quarter-chord line of their respective surfaces. The average chordwise center of pressure for loads due to the rudder was estimated to be the 0.48 chord from the pressure-distribution data given in reference 14. Although no pressure-distribution data were available for the specific wing-aileron plan form, the center of pressure for the aileron loads was estimated to be at the 0.58 chord from an examination of pressure distributions on similar swept-wing plan forms. Fuselage influence coefficients used in the analysis were obtained from data given in references 15 and 16 and are listed in table III together with the wing influence coefficients which were obtained from reference 12. Wing stations and equivalent weights used in the analysis are shown in figure 13. An example of the application of the method to obtain the effect of wing deflections on the derivative C_{l_β} is given in Appendix B. Predicted aerodynamic derivatives for both the flexible and rigid conditions are listed in table V.

TABLE V.—PREDICTED LATERAL-DIRECTIONAL STABILITY DERIVATIVES FOR THE FLEXIBLE AND RIGID AIRPLANE AT AN ALTITUDE OF 35,000 FEET; W=115,000 POUNDS

Quantity	Flexible				Rigid			
M	0. 5	0. 6	0. 7	0. 8	0. 5	0. 6	0. 7	0. 8
q	87. 2	125. 5	171. 0	223. 1	87. 2	125. 5	171. 0	223. 1
C_L	. 922	. 642	. 471	. 361	. 922	. 642	. 471	. 361
C_{l_p}	−. 430	−. 429	−. 427	−. 426	−. 490	−. 507	−. 540	−. 570
C_{n_p}	−. 0960	−. 0660	−. 0470	−. 0350	−. 0994	−. 0692	−. 0507	−. 0389
C_{l_r}	. 215	. 136	. 090	. 060	. 264	. 184	. 135	. 104
C_{n_r}	−. 142	−. 137	−. 134	−. 130	−. 150	−. 150	−. 150	−. 150
C_{l_β}	−. 170	−. 141	−. 122	−. 112	−. 157	−. 129	−. 113	−. 101
C_{n_β}	. 110	. 106	. 102	. 098	. 120	. 120	. 120	. 120
C_{Y_β}	−. 575	−. 566	−. 555	−. 544	−. 600	−. 600	−. 600	−. 600
$C_{l_{\delta_r}}$	. 0052	. 0090	. 0109	. 0122	. 0057	. 0095	. 0119	. 0135
$C_{n_{\delta_r}}$	−. 0724	−. 0700	−. 0672	−. 0645	−. 0778	−. 0778	−. 0778	−. 0778
$C_{Y_{\delta_r}}$	. 183	. 180	. 175	. 171	. 194	. 194	. 194	. 194
$C_{l_{\delta_a}}$	. 0594	. 0528	. 0462	. 0392	. 0770	. 0770	. 0770	. 0770
$C_{n_{\delta_a}}$	−. 0103	−. 0064	−. 0041	−. 0027	−. 0133	−. 0093	−. 0068	−. 0052
r_X	−. 116	−. 059	−. 005	. 031	−. 103	−. 047	−. 010	. 014
r_Z	−. 048	−. 021	−. 005	. 007	−. 047	−. 020	−. 005	. 007

TRANSFER-FUNCTION COEFFICIENTS

Transfer functions obtained by solving the three-degree-of-freedom equations are presented in Appendix D. As noted in this appendix, some of the transfer functions may be simplified for the frequency range of interest. After the spiral mode is neglected, rolling response to aileron becomes

$$\frac{p}{\delta_a}=\frac{A_3(D^2+a_1D+a_2)}{(D+D_r)(D^2+c_1D+c_2)} \tag{19}$$

The transfer function may also be written as

$$\frac{p}{\delta_a}=\frac{K_{p/\delta_a}[1+2\zeta_a D/\omega_a+(D/\omega_a)^2]}{(1+TD)\left[1+2\zeta_{DR}D/\omega_{n_{DR}}+(D/\omega_{n_{DR}})^2\right]} \tag{20}$$

For yawing and sideslipping response to rudder motion, both spiral and rolling modes may be neglected so that

$$\frac{r}{\delta_r}=\frac{H_rD}{D^2+c_1D+c_2} \tag{21}$$

$$\frac{\beta}{\delta_r}=\frac{J_\beta}{D^2+c_1D+c_2} \tag{22}$$

These quantities may also be expressed as

$$\frac{r}{\delta_r}=\frac{K_{r/\delta_r}D}{1+2\zeta_{DR}D/\omega_{n_{DR}}+(D/\omega_{n_{DR}})^2} \tag{23}$$

$$\frac{\beta}{\delta_r}=\frac{K_{\beta/\delta_r}}{1+2\zeta_{DR}D/\omega_{n_{DR}}+(D/\omega_{n_{DR}})^2} \tag{24}$$

The predicted frequency responses may be obtained from the transfer functions after $i\omega$ is substituted for the operator D. The conversion of numerator transfer-function coefficients from stability to body axes for comparison with frequency responses measured with respect to body axes is given in Appendix D.

APPROXIMATE EQUATIONS TO OBTAIN AERODYNAMIC DERIVATIVES FROM TRANSFER-FUNCTION COEFFICIENTS

The equations for the aerodynamic derivatives were obtained as follows: The coefficients C_3, C_2, and C_1 of the char-

acteristic equation given in Appendix D were expressed in terms of their principal aerodynamic derivatives. The coefficients were also expressed in terms of the factors of the characteristic equation D_r, c_1, and c_2. By equating the coefficients of like powers of D, three simultaneous equations were obtained with three unknowns, L_p, N_r+Y_β, and N_β'. A cubic equation for L_p was then obtained by eliminating the other unknowns. The derivative L_p was found by using an approximate solution for a cubic equation together with an approximate equation for the amplitude of the roll to yaw ratio of the Dutch roll mode, $\left|\frac{p}{r}\right|$. Equations for the two other derivatives could then be obtained. The equations are

$$L_p=-D_r-\mu \tag{25}$$

$$N_r+Y_\beta=\mu-c_1 \tag{26}$$

$$N_\beta'=c_2+\mu(D_r-c_1) \tag{27}$$

where

$$\mu=\frac{\left|\frac{p}{r}\right|(N_p-Y_\phi-D_r r_Z)}{\sqrt{1+D_r^2/c_2}} \tag{28}$$

Note that these equations correspond to those given in reference 3 except for the quantity μ. The additional term μ could be considered as a measure of the coupling between the Dutch roll and rolling modes. The equation used for L_β' was obtained from reference 3

$$L_\beta'=\left|\frac{p}{r}\right| N_\beta'\sqrt{1+L_p^2/c_2} \tag{29}$$

Approximate relations for control effectiveness were obtained by substituting typical numerical values in the equations given in Appendix D, and the following expressions (analogous to those given in ref. 3) were found to be valid for the present airplane. The rudder effectiveness derivative was obtained from

$$N_{\delta_r}=H_r \text{ or } -J_\beta \tag{30}$$

while aileron effectiveness was obtained from

$$L_{\delta_a}=A_3 \tag{31}$$

Aerodynamic derivatives may be found from the quantities on the left-hand side of equations (25) through (31) through use of the definitions given in the notation.

Thus the aerodynamic derivatives may be obtained from transfer-function coefficients matched from experimental data, provided that an estimate is made of the product of inertia, the derivative C_{n_p}, and also the effective moments of inertia for the flexible airplane. Estimated variations in effective inertia characteristics are presented in figure 20. The principal effect of flexibility is to reduce the rolling moment of inertia. This effect is largely due to the mass of the wing-mounted nacelles. In order to demonstrate the adequacy of the approximate equations, predicted transfer-

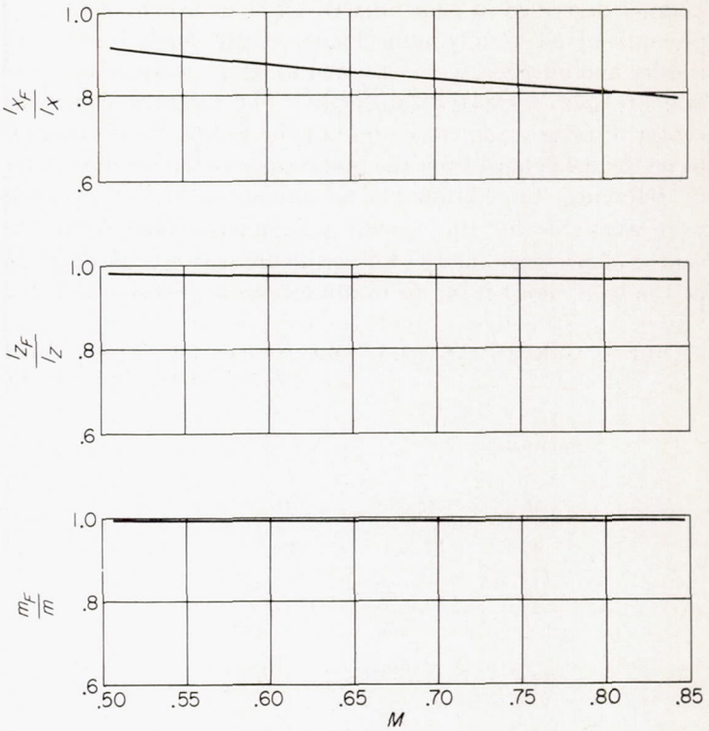

FIGURE 20.—Influence of flexibility on effective lateral-directional inertia characteristics.

function coefficients were first calculated from the predicted derivatives (table V) using the complete expressions for the transfer-function coefficients. Then approximate values of the derivatives were calculated from the predicted transfer-function coefficients using equations (25) to (29), and also using the equations with $\mu=0$, which correspond to the equations given in reference 3. Comparisons of these derivatives are shown in figure 21. Also shown are derivatives calculated from equations given in reference 3. In all cases the values of derivatives using the approximate equations are closer to the estimated values than those obtained using the equations from reference 3. This is particularly true for the derivative, $C_{n_r}+2K_Z^2C_{Y_\beta}$. Although not shown, a similar comparison was made for the rigid case, and the inclusion of the quantity μ also improved the agreement with the predicted derivatives.

MEASURED RESPONSES AND COMPARISON WITH PREDICTED RESPONSES

FREQUENCY RESPONSES

In the discussion that follows, effects of the relatively low frequency lateral-directional modes will be investigated first. Comparisons will be made between measured and predicted responses to determine the frequency range for which the predictions are adequate. Then the higher frequency structural modes will be discussed and compared with values obtained from the ground oscillation tests of reference 9. The frequency-response data to be presented include: measured frequency responses to aileron and rudder inputs over a fairly wide Mach number range (figs. 22 and 23), typical comparisons of measured responses at the center of gravity and tail (figs. 24 and 25), and typical comparisons

of measured and estimated frequency responses (figs. 26 and 27).

Lateral-directional modes.—The ailerons excite principally the rolling mode as well as some Dutch roll mode as shown in the roll-rate response (fig. 22 (a)), which is seen to be of the same form as that indicated in equation (20). The rolling mode (a first-order term) causes the net shift of 90° in the phase angle between the frequencies of 0.5 to 5 radians per second and the slope of the amplitude curve in the frequency range of 2 to 7 radians per second, while the peak in the amplitude curve that occurs at frequencies from about 1 to 1.5 radians per second is due to the Dutch roll mode (a second-order term). Responses in sideslip and yaw rate are quite small (figs. 22 (b) and 22 (c)). The rudder mainly excites the Dutch roll mode (fig. 23). For both inputs, differences in tail and center-of-gravity roll and yaw rates are small in this frequency range. This may also be seen from the time histories (figs. 4 and 5).

The predicted results for the flexible airplane in general agree reasonably well with experimental results for frequencies up to about 3 to 8 radians per second, with the possible exception of wing-tip acceleration (figs. 26 (e) and 27 (f)). Also some discrepancies are apparent in the lowest frequency range (near 0.5 radian/sec) which is the region in which the experimental frequency-response accuracy obtained from pulse-type inputs becomes relatively poor, as was discussed in the section Reduction of Transient Data to Frequency Response. For the aileron responses, the predicted gain for the flexible case is much lower than that for the rigid, reflecting the reduction in aileron effectiveness. However, the p/δ_r responses (fig. 27 (a)) indicate a higher gain for the flexible case. This is largely due to the higher value of the ratio of C_{l_β} to the effective moment of inertia in the flexible case. Flexibility also reduces the frequency and damping of the Dutch roll mode. A discrepancy between theory and experiment in the curves for r/δ_a (fig. 26 (b)) is that the experimental phase angles shift 180° while the predicted values approach a 360° shift. One possible explanation is that the smaller phase shift could have been obtained from the predicted curve if a more negative value of $C_{n_{\delta_a}}$ had been assumed. A structural mode could also affect the phase angle in this region.

Structural modes.—A peak occurs in all the frequency responses to aileron (fig. 22) at about 13.4 radians per second which will be called the first wing antisymmetric bending mode. This compares with 14.4 radians per second obtained from ground vibration tests (ref. 9). The mode is particularly noticeable in the center-of-gravity roll rate and wing-tip acceleration responses. In the time history for the wing optigraph, this mode is seen to predominate. Another point of interest is that the amplitude of the yaw rate at the tail is greater than that for the center of gravity, as may be seen from both the frequency-response and time-history curves. The mode frequency remains essentially constant for the flight range investigated although there is a slight increase in amplitude with Mach number. Measurements of the time history indicated that the damping was also essentially constant over the flight range at a value of about 0.025 critical.

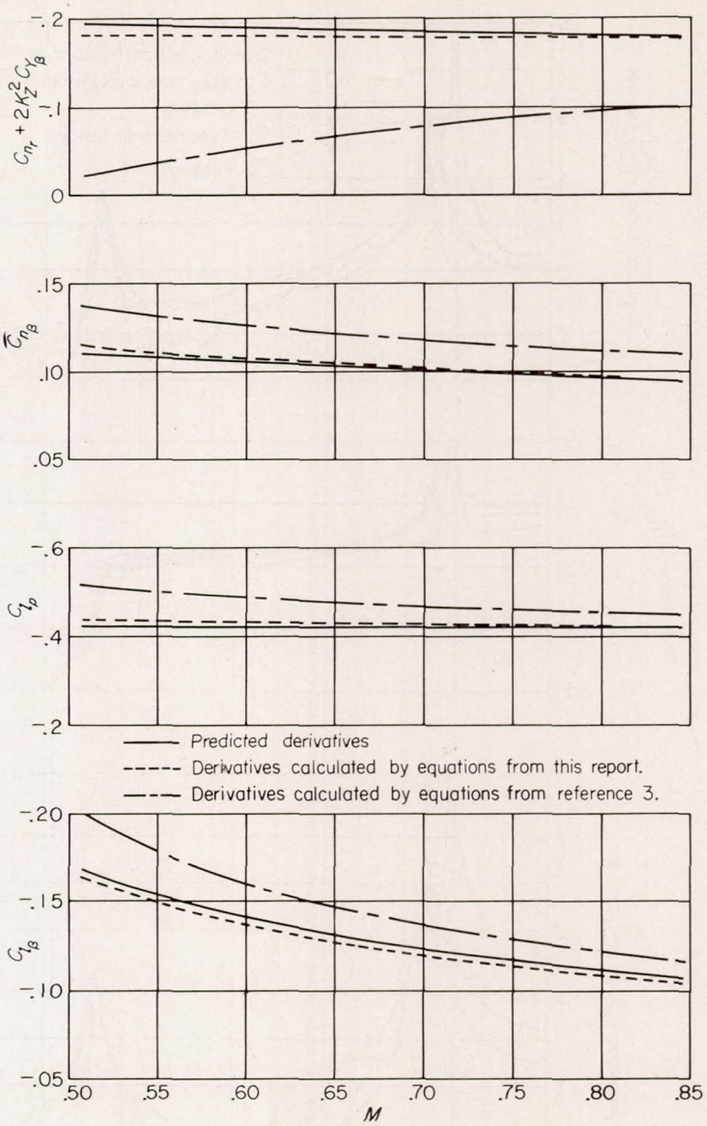

FIGURE 21.—Comparison of predicted lateral-directional stability derivatives for the flexible airplane with those calculated from predicted transfer-function coefficients using approximate equations.

The shape of this mode, obtained from measurements of the free oscillation amplitudes of the accelerometer and turn-meter traces resulting from aileron inputs, is shown in figure 28. When the curve was determined, small corrections for chordwise displacement of the instruments were made where necessary to transfer the accelerometer results to the 17-percent and 58-percent chord lines corresponding to the front and rear spars, respectively. In the placement of pickups for an autopilot system, it is desirable to locate them at points on the structure that are least affected by the structural modes in order to avoid introducing undesired signals. For a roll gyro, the optimum location for minimizing the angular velocity input of the antisymmetric wing mode would be where the wing mode shape has zero slope which, as shown in figure 28, is at $\eta=0.38$ near the inboard nacelle, while for a linear accelerometer, the optimum location would be at a nodal point, which in figure 28 is at η of about 0.55 just outboard of the nacelle. The wing accelerometer node line obtained from the two span positions

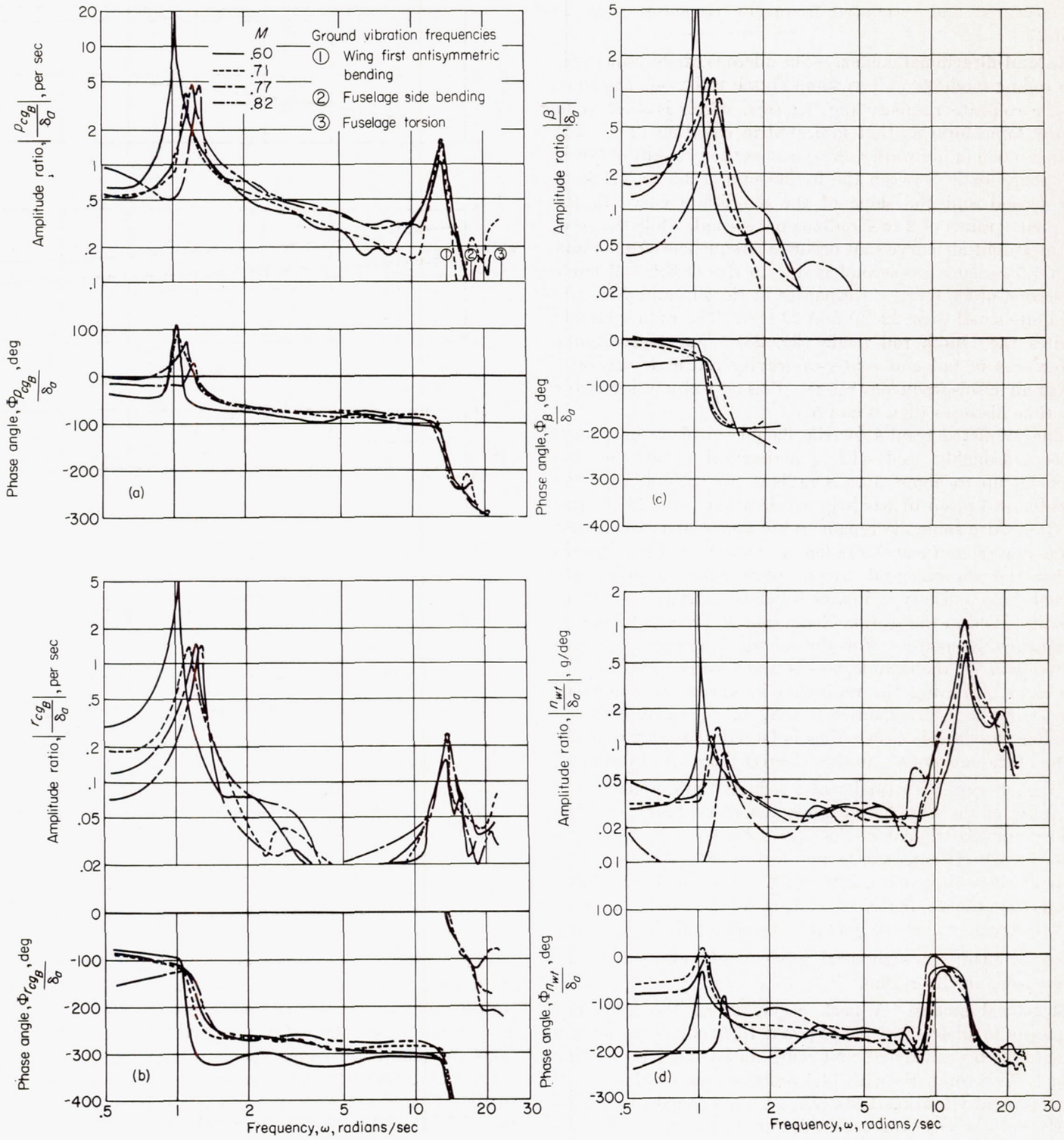

(a) Rolling velocity at the center of gravity.

(b) Yawing velocity at the center of gravity.

(c) Sideslip angle.

(d) Wing-tip acceleration.

FIGURE 22.—Frequency responses to aileron inputs at various Mach numbers.

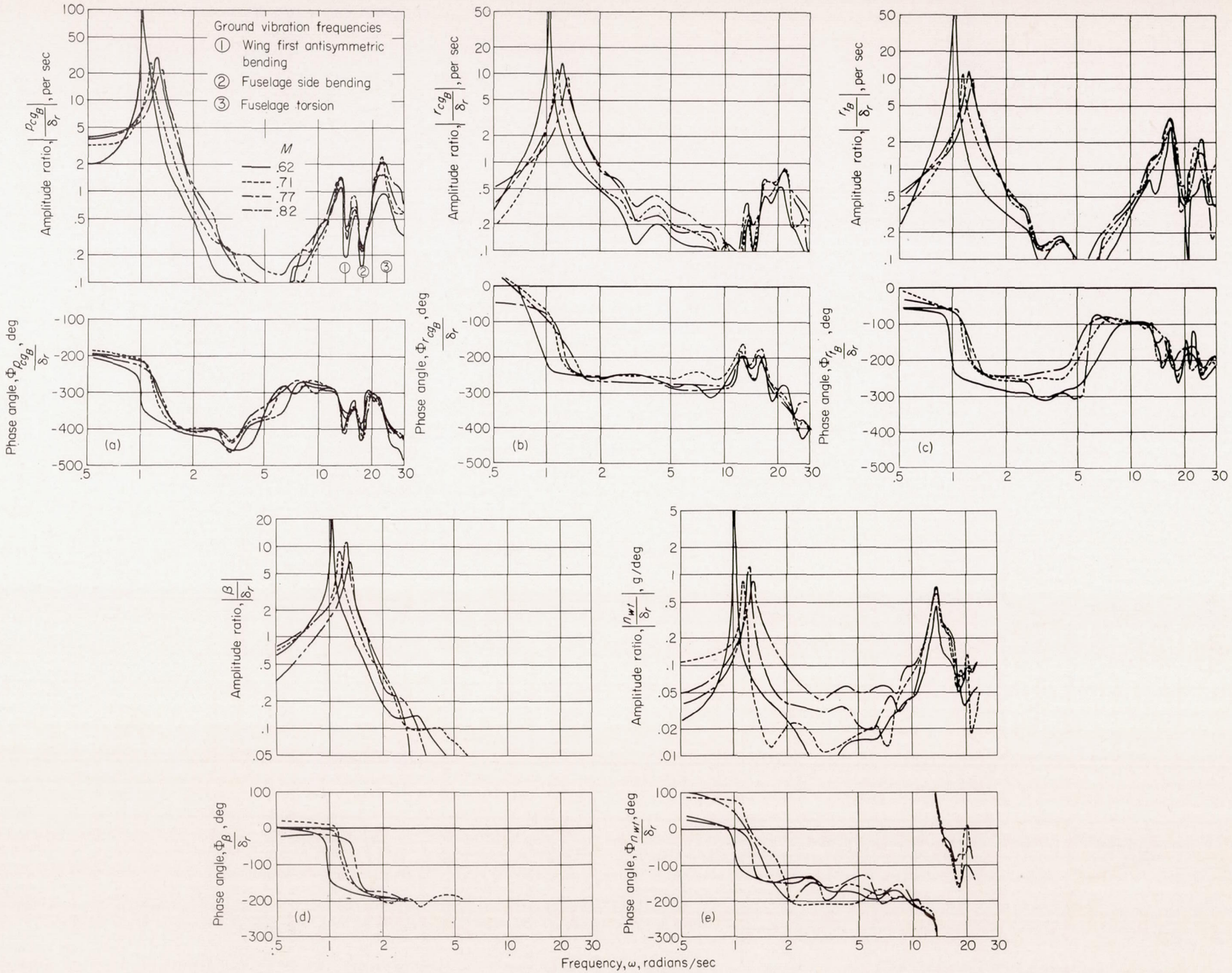

(a) Rolling velocity at the center of gravity. (b) Yawing velocity at the center of gravity. (c) Yawing velocity at the tail.
(d) Sideslip angle. (e) Wing-tip acceleration.

FIGURE 23.—Frequency responses to rudder inputs at various Mach numbers.

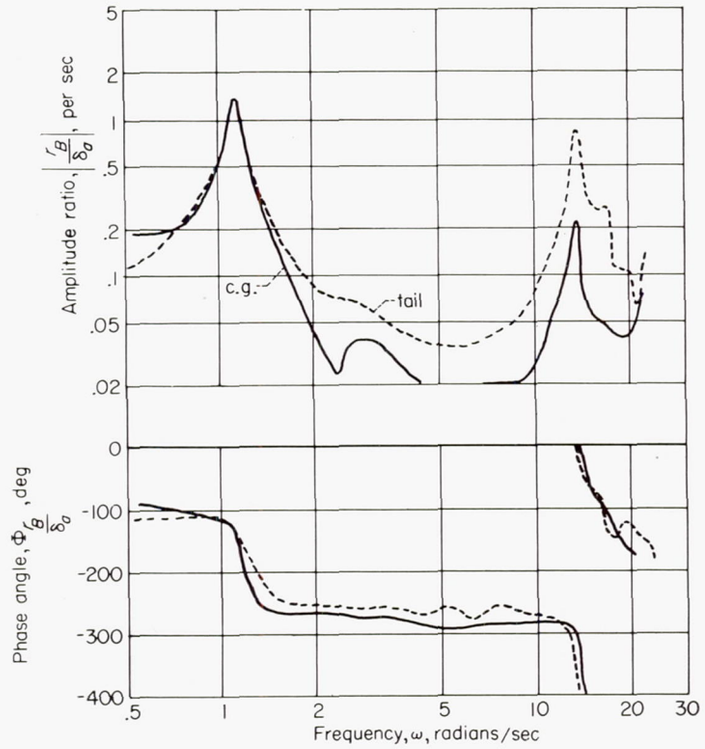

FIGURE 24.—Comparison of the measured yawing velocity frequency responses at the center of gravity and the tail to an aileron input; $M=0.71$.

shows good agreement with that obtained from ground vibration tests.

In the wing-tip acceleration curve (fig. 22 (d)), a dip in the amplitude and a shift of approximately 180° in the phase angle relative to the center-of-gravity roll rate (fig. 22 (a)) occurs in a frequency range somewhat lower than the wing bending frequency. This motion can be illustrated as follows: At low frequencies, the relation between wing bending and roll angle is as shown in the following sketch. As the frequency increases, the amount of wing

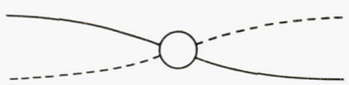

bending relative to roll angle becomes greater so that the acceleration at the tip reverses sign with respect to the roll angle as shown in the next sketch. This trend continues

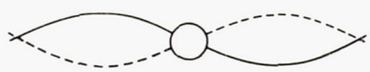

until the bending frequency is reached.

An examination of figure 22 shows that no additional modes were excited to any appreciable extent in the measured frequency range above that of the wing first antisymmetric bending mode, although two modes were measured from ground vibration tests (ref. 9).

While the rudder pulses also excite the wing antisymmetric bending mode, their principal effect is to excite two slightly higher frequency modes which are predominantly

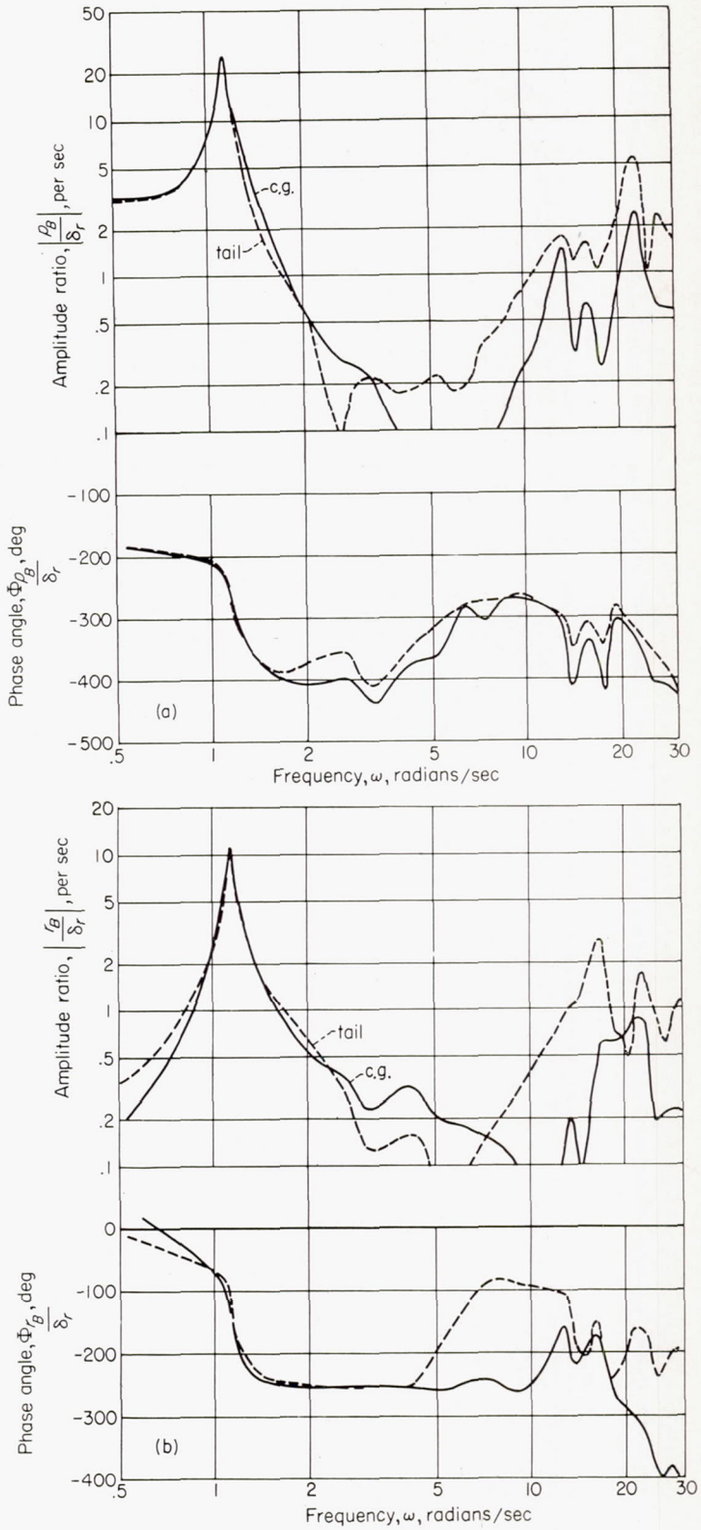

(a) Rolling velocity.
(b) Yawing velocity.

FIGURE 25.—Comparison of measured frequency responses at the center of gravity and the tail to a rudder input; $M=0.71$.

fuselage modes as may be seen from the responses of yaw and roll rate at the tail and center of gravity (figs. 23 and 25). The lower frequency, which is predominantly fuselage side bending, is 16.5 radians per second while the upper frequency, which is principally fuselage torsion, is 23 radians

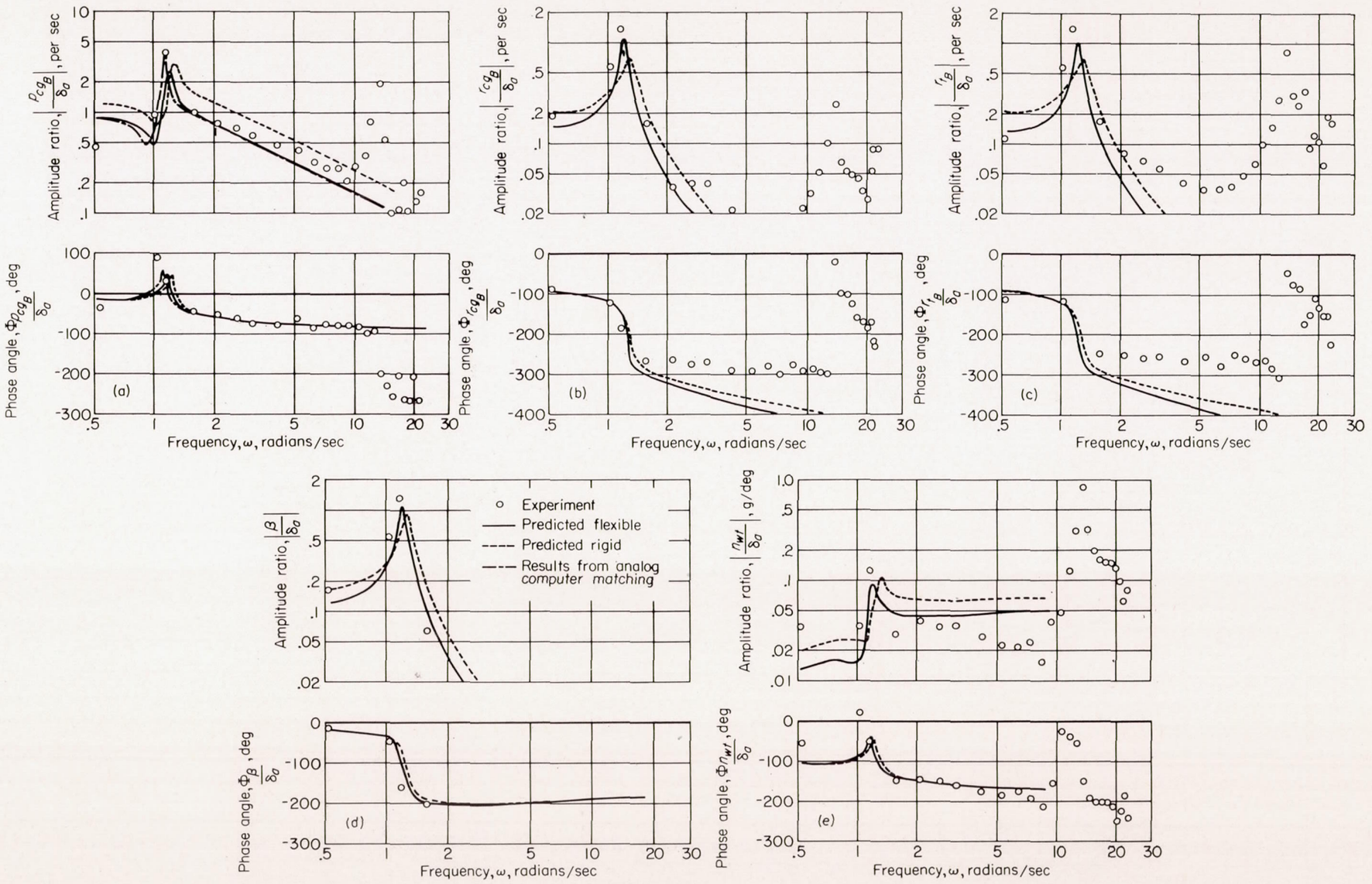

(a) Rolling velocity at the center of gravity. (b) Yawing velocity at the center of gravity. (c) Yawing velocity at the tail. (d) Sideslip angle. (e) Wing-tip acceleration.

FIGURE 26.—Comparison of experimental and predicted frequency responses to aileron input; $M=0.71$.

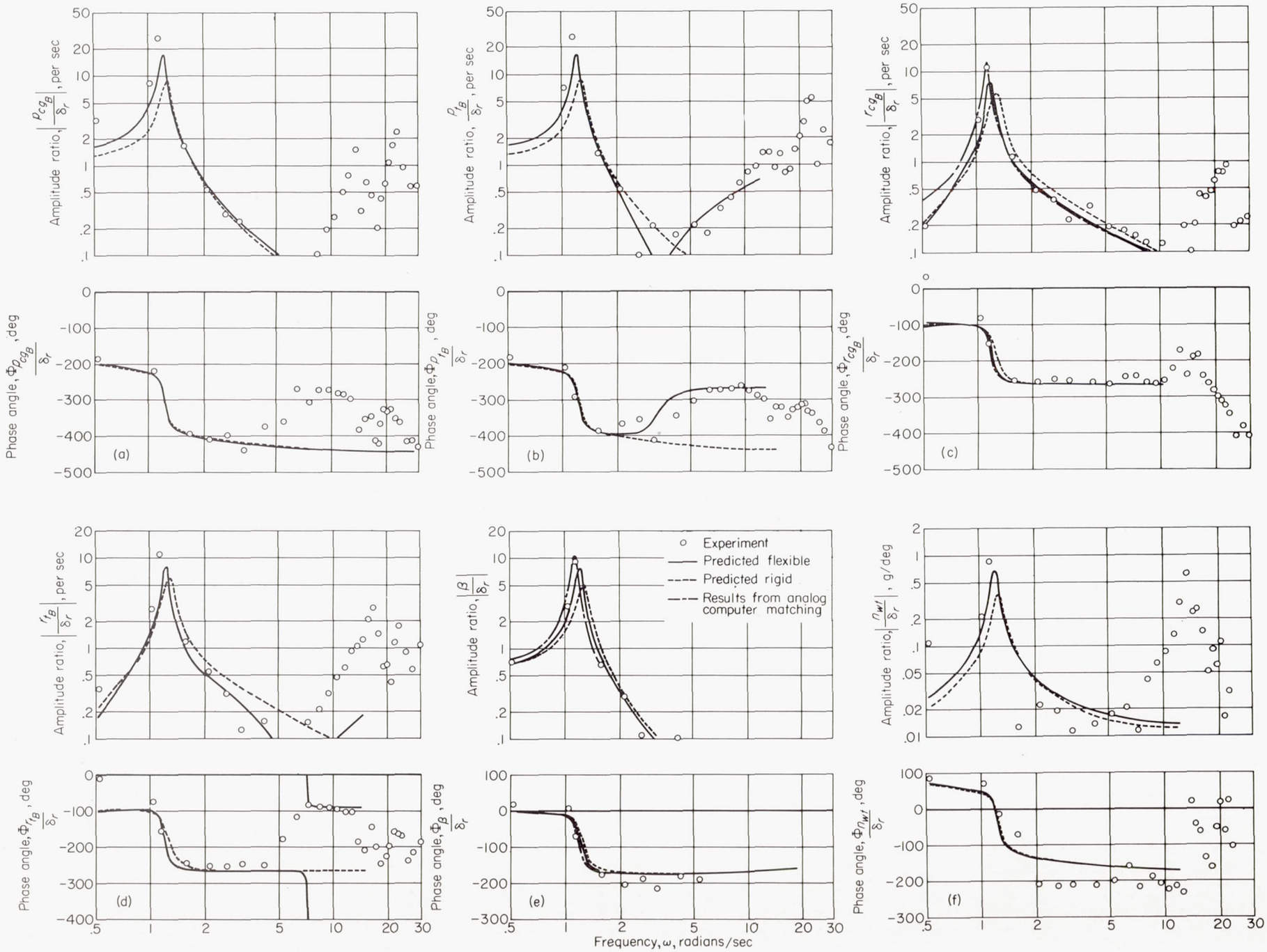

(a) Rolling velocity at the center of gravity. (b) Rolling velocity at the tail. (c) Yawing velocity at the center of gravity.
(d) Yawing velocity at the tail. (e) Sideslip angle. (f) Wing-tip acceleration.

FIGURE 27.—Comparison of experimental and predicted frequency responses to rudder input; $M=0.71$.

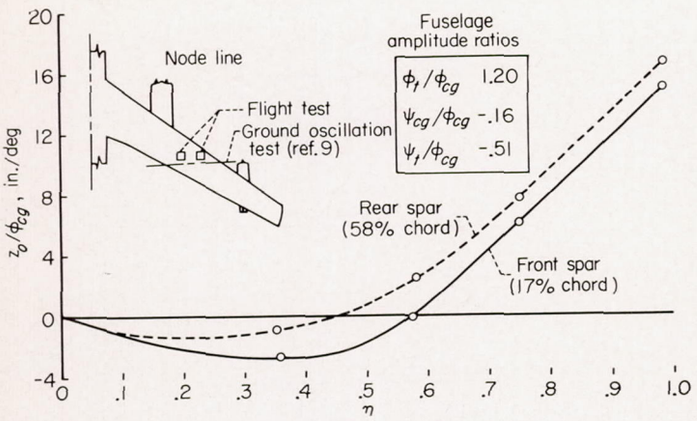

FIGURE 28.—First antisymmetric wing bending free oscillation mode shape; $M=0.71$.

per second. These frequencies compare with ground vibration test values of 18.0 and 24.5 radians per second, respectively (ref. 9). The prominence of these modes at the tail may also be seen from the transient responses due to the rudder input (fig. 5).

The frequency responses for roll and yaw rate at the tail due to a rudder pulse (fig. 25) also indicate regions of low amplitude at frequencies below the structural natural frequencies (about 3 to 8 radians per second). While phase angle for the tail yaw rate shifts 180° out of phase with that of the center of gravity, as was the case for the wing at frequencies below that of the antisymmetric bending mode, the phase angle shifts for the tail and center-of-gravity roll rate are approximately the same so that they remain in phase. It is of interest to note that by the inclusion of only the pseudostatic effects of sideslip, yawing acceleration, etc., on the tail deflections, these amplitude and phase-angle trends are predicted (figs. 27 (b) and 27 (d)). While the direction of the 180° phase-angle shift does not agree for the tail yaw rate, the resultant shift is the same. Since the amplitude ratio is quite low in this region, some question does exist as to the direction of the phase-angle shifts for both the experimental and predicted values.

TRANSFER-FUNCTION COEFFICIENTS

Transfer-function coefficients of the simplified transfer functions for p/δ_a, r/δ_r, and β/δ_r described in a previous section were obtained by matching the response time histories (e. g., figs. 4 and 5) by means of an analog computer. They were then converted from body axes to stability axes. In some cases, small residual oscillations, which were principally due to the lightly damped Dutch roll mode, were present when the airplane control pulse was applied. Initial conditions were applied to the simulator to include this motion, although in all cases this had only a small effect on transfer-function coefficients. In matching the time histories of p/δ_a on the analog computer, it was found convenient to represent the third-order transfer function by parallel networks of first-order and second-order transfer functions. This representation is equivalent to separating the third-order transfer function into the partial fraction form shown in Appendix D. In this way contributions of the Dutch roll and rolling modes to the resultant motions could be matched separately.

Comparisons of experimentally determined transfer-function coefficients with predicted values (with respect to stability axes) for both the flexible and rigid case based on the simplified transfer functions (eqs. (20), (23), and (24)) are shown in figure 29. In general, agreement between experiment and theory for both numerator and denominator is seen to be good, as was the case reported in reference 17 for 25,000 feet.

For the denominator terms, the values of measured damping ratio are an average of 0.015 less than the estimated flexible values. While the ratios of measured to estimated values are relatively large, the average magnitude is approaching zero at the lower values of Mach number, and hence the discrepancy is considered to be small. Also some scatter occurred in the time constant T. This parameter was difficult to evaluate because it did not have as important an effect on the transient response to a pulse as did the other parameters. Flexibility is seen to reduce both the frequency and damping of the Dutch roll mode. These reductions are caused primarily by the decrease in vertical-tail effectiveness due to fuselage and tail flexibility having a larger effect than the decrease in effective yawing moment of inertia. Flexibility changes the time constant T very little. This term depends principally on the ratio of effective rolling moment of inertia to the aerodynamic damping in roll. Since the rolling moment of inertia is due largely to the nacelle and wing weights, wing flexibility reduces both the aerodynamic and inertia loads by about the same amount.

For the numerator terms also, good agreement is obtained between theory and experiment. The scatter that occurred in the measured values of ζ_a resulted from the small effect of ζ_a on the time histories matched with the analog computer. The comparison of the matched curves in figures 4 and 5 with the measured time histories indicates that the transfer functions corresponding to the Dutch roll mode only for the rudder pulses, and the rolling and Dutch roll modes for the aileron pulses were sufficient to define the time histories adequately. The greatest effect of flexibility is seen to be in the reduction in gain for p/δ_a. This reflects the reduction in aileron effectiveness associated with outboard ailerons. The predicted values of ζ_a and ω_a are slightly different from ζ_{DR} and $\omega_{n_{DR}}$ and approach these quantities at the higher Mach numbers. These differences depend upon the aerodynamic derivatives that affect the quantities μ and $C_{n_{\delta_a}}$, which become relatively small at the higher Mach numbers and corresponding low angles of attack. These effects are reflected in the time histories by the amount of excitation of the Dutch roll mode and also by a reduction in over-all gain. For the limiting case of $\zeta_a=\zeta_{DR}$ and $\omega_a=\omega_{n_{DR}}$, effects of the Dutch roll mode are eliminated and the transfer function (eq. (20)) reduces to a first-order form.

AERODYNAMIC DERIVATIVES

Generally good agreement is obtained between predicted and experimental values of the aerodynamic derivatives (fig. 30). Differences between predicted aerodynamic derivatives for the flexible and rigid cases are generally somewhat greater than the differences between transfer-function coefficients since the latter are partially compensated by

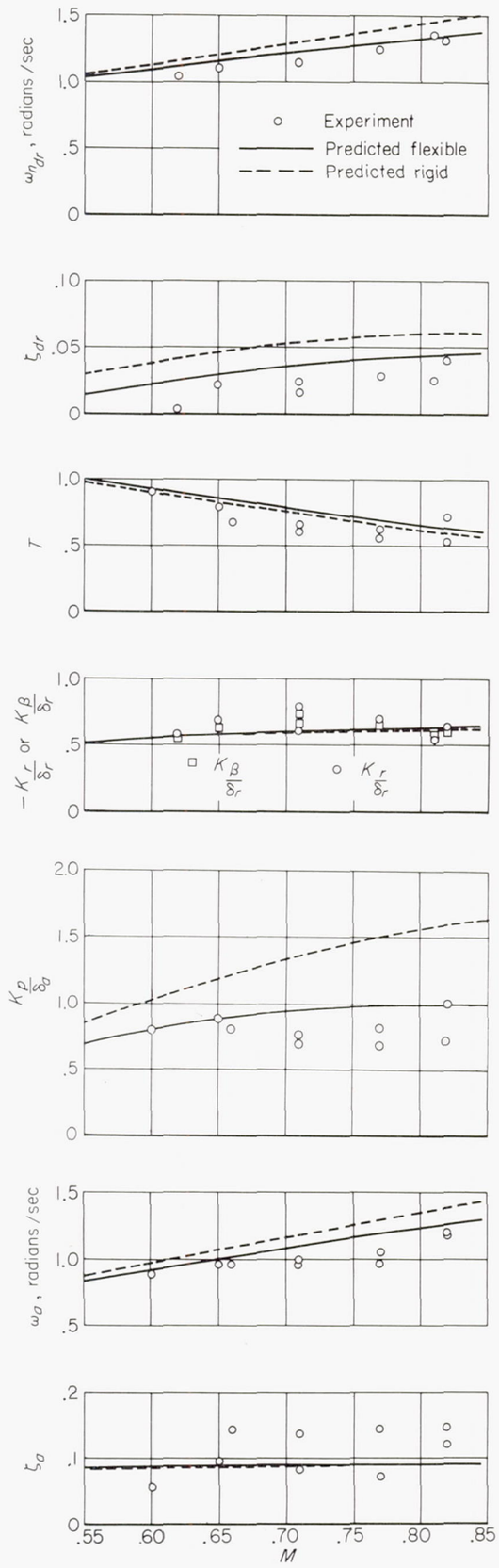

FIGURE 29.—Comparison of experimental and predicted lateral-directional transfer-function coefficients.

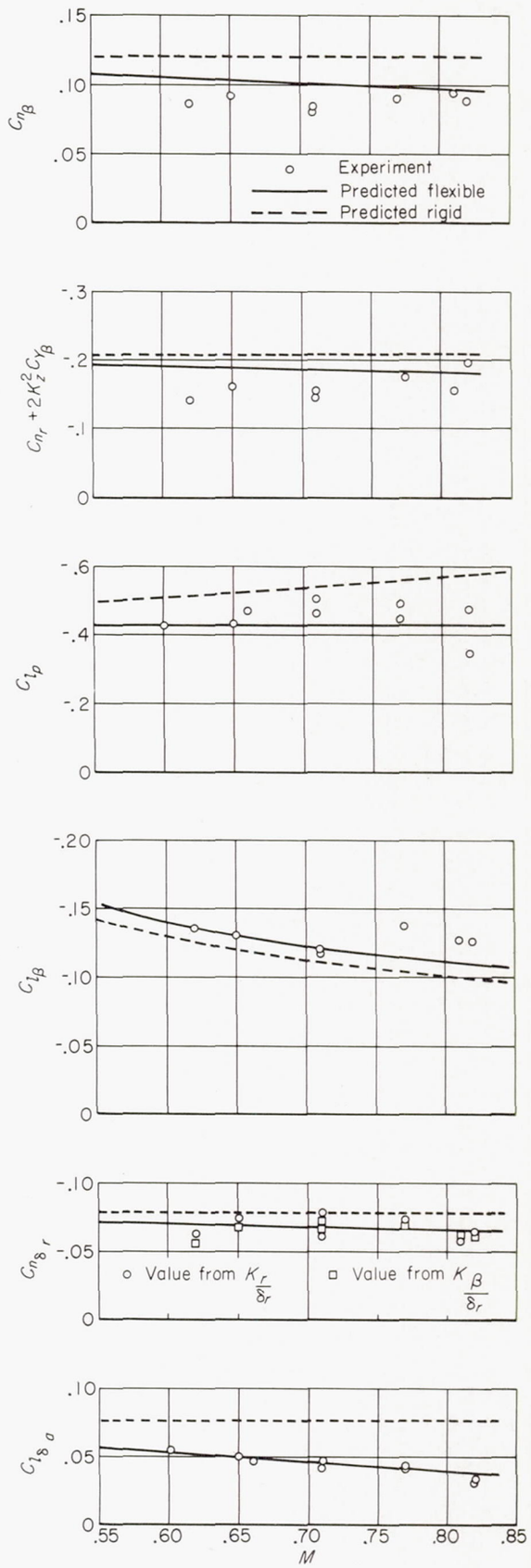

FIGURE 30.—Comparison of experimental and predicted lateral-directional stability derivatives.

changes in the effective moments of inertia due to flexibility. In general, flexibility tends to reduce the values of the aerodynamic derivatives with the largest reduction occurring for $C_{l_{\delta_a}}$ and C_{l_p}. However, flexibility tends to increase the magnitude of C_{l_β} since the usual decrease in value of a derivative due to flexibility is more than compensated by the increase in dihedral due to wing lift.

CONCLUSIONS

The evaluation of the dynamic response of a large flexible airplane to elevator, aileron, and rudder pulses at 35,000 feet over a Mach number range of 0.6 to 0.85 and the comparisons with predicted response have led to the following conclusions:

1. The pulse technique provided dynamic-response data which were sufficiently accurate for evaluation of frequency response from 1 to 25 radians per second. This frequency range includes the relatively low frequency longitudinal short-period, Dutch roll, and rolling modes, as well as the higher frequency structural modes, wing first symmetric bending, wing first antisymmetric bending, fuselage vertical bending, fuselage side bending, and fuselage torsion modes.

2. Predicted longitudinal and lateral-directional responses based on rigid airplane equations with coefficients modified to include zero-frequency aeroelastic effects were in good agreement with measured responses for frequencies below one-half of the lowest structural mode natural frequency.

3. For longitudinal responses, the principal effect of airplane flexibility is to decrease the natural frequency of the short-period mode, a trend which may be attributed principally to fuselage and tail bending and the associated loss in the angle-of-attack moment derivative, C_{m_α}. This C_{m_α} effect would be more significant and have a larger effect on the steady maneuvering acceleration per unit elevator deflection if it were not for the compensating effect of deflections due to inertial loads.

4. The principal effect of flexibility on the lateral-directional response is the reduction in gain of airplane response to aileron motion, reflecting the reduction in aileron effectiveness, and also a reduction in damping and frequency of the Dutch roll mode.

5. The principal lateral-directional and control-effectiveness derivatives evaluated with approximate equations were in good agreement with predicted derivatives when zero-frequency effects of flexibility were included.

6. For frequencies near and above the natural frequencies of structural modes, the modified equations for zero-frequency effects of flexibility were inadequate. However, near the natural frequency of a structural mode, the response amplitude varies considerably with location on the airplane, and it appears that for some locations, at least, the response near the structural mode frequency would be the same as predicted by the simplified equations.

7. The frequencies of the structural modes measured in flight were within about 10 percent of the frequencies of the corresponding modes measured in ground vibration tests.

8. The method of employing aerodynamic and structural influence coefficients in the aeroelastic calculations proved to be advantageous in simplifying spanwise loading calculations and in applying static test load data.

AMES AERONAUTICAL LABORATORY
NATIONAL ADVISORY COMMITTEE FOR AERONAUTICS
MOFFETT FIELD, CALIF., *Aug. 6, 1957*

APPENDIX A

NOTATION

A	aspect ratio
C_L	lift coefficient
C_l	rolling-moment coefficient
C_m	pitching-moment coefficient
C_n	yawing-moment coefficient
C_Y	side-force coefficient
D	differential operator, $\frac{d}{dt}$
I_X	moment of inertia about the X axis, slug-ft^2
I_{X_F}	effective rolling moment of inertia for flexible airplane, $I_X - q_o S b C_{l_{\ddot{\varphi}}}$, slug-ft^2
I_Z	moment of inertia about the Z axis, slug-ft^2
I_{Z_F}	effective yawing moment of inertia for flexible airplane, $I_Z - q_o S b C_{n_{\ddot{\psi}}}$, slug-ft^2
I_{XZ}	product of inertia, slug-ft^2
K_y	dimensionless radius of gyration about principal lateral axis, mean aerodynamic chords
K_Z	dimensionless radius of gyration about principal normal axis, wing spans
K_n	gain of $\frac{n}{\delta_e}$ transfer function
K_{p/δ_a}	gain of simplified $\frac{p}{\delta_a}$ transfer function
K_{r/δ_r}	gain of simplified $\frac{r}{\delta_r}$ transfer function
K_{β/δ_r}	gain of simplified $\frac{\beta}{\delta_r}$ transfer function
$K_{\dot{\theta}}$	gain of $\frac{\dot{\theta}}{\delta_e}$ transfer function
M	Mach number
S	wing area, sq ft
T	rolling-mode time constant, sec
T_n	normal acceleration time constant, sec
$T_{\dot{\theta}}$	pitching velocity time constant, sec
V	velocity, ft/sec
W	gross weight of airplane, lb
b	wing span, ft
c	local chord of wing measured parallel to the plane of symmetry
$c.g.$	center of gravity, percent $\overline{c}$
$\overline{c}$	wing mean aerodynamic chord, $\frac{2}{S}\int_o^{b/2} c^2 dy$
c_l	section lift coefficient
g	acceleration due to gravity, 32.2 ft/sec^2
i	$\sqrt{-1}$
m	mass of airplane, slugs
m_F	effective mass for lateral acceleration of flexible airplane, $m - \frac{q_o S}{V} C_{Y_{\dot{\beta}}}$
n	normal acceleration, positive downward, gravity units
p	rolling velocity, radians/sec
q	dynamic pressure, lb/sq in.
q_o	dynamic pressure, lb/sq ft
r	yawing velocity, radians/sec
t	time, sec
$x_{(\ )}$	longitudinal distance from center of gravity to subscript quantity, positive when center of gravity is forward of subscript quantity, ft
y	spanwise coordinate perpendicular to plane of symmetry, ft
z	structural deflection, positive downward, in.
z_o	vertical coordinate, positive downward, in.
α	angle of attack, radians
β	angle of sideslip, radians (except as otherwise noted)
δ_a	total aileron deflection, measured in a plane perpendicular to the hinge line, positive right aileron up, radians (except as otherwise noted)
δ_e	elevator deflection, positive downward, radians (except as otherwise noted)
δ_r	rudder deflection, measured in a plane perpendicular to the hinge line, positive trailing edge left, radians (except as otherwise noted)
ϵ	change in streamwise angle of attack due to wing distortion, radians
ζ	damping ratio, dimensionless
ζ_a	damping ratio of numerator term of $\frac{p}{\delta_a}$ transfer function
η	spanwise coordinate, wing semispans
θ	pitch angle, radians
μ	parameter used in evaluating aerodynamic derivatives from transfer-function coefficients, defined in equation (28)

ρ	mass density of air, slugs/cu ft
τ	$\frac{m}{\rho SV}$, sec
φ	angle of bank, radians
$\Phi_{\left(\frac{\text{output}}{\text{input}}\right)}$	phase angle of output quantity minus phase angle of input quantity
ψ	angle of yaw, radians
ω	frequency, radians/sec
ω_a	undamped natural frequency of numerator term of $\frac{p}{\delta_a}$ transfer function
ω_n	undamped natural frequency, radians/sec
C_{L_α}, $C_{L_{\dot{\alpha}}}$, $C_{L_{\dot{\theta}}}$, $C_{L_{\ddot{\theta}}}$, C_{L_δ}, C_{m_α}, $C_{m_{\dot{\alpha}}}$, $C_{m_{\dot{\theta}}}$, $C_{m_{\ddot{\theta}}}$, C_{m_δ}, C_{l_β}, C_{n_β}, $C_{l_{\dot{\delta}}}$, $C_{n_{\dot{\delta}}}$, $C_{n_{\dot{\beta}}}$, C_{Y_β}, $C_{Y_{\dot{\beta}}}$, $C_{Y_{\dot{\psi}}}$, C_{Y_δ}, C_{Y_φ}, $C_{n_{\dot{\psi}}}$, $C_{l_{\ddot{\varphi}}}$, $C_{l_{\ddot{\psi}}}$, $C_{n_{\ddot{\psi}}}$	derivative of coefficient with respect to subscript
C_{l_r}, C_{n_r}, C_{l_p}, C_{n_p}	derivative of coefficient with respect to subscript$\times\frac{b}{2V}$
L_p	$\frac{q_o Sb^2}{2VI_{X_F}} C_{l_p}$, per sec
L_r	$\frac{q_o Sb^2}{2VI_{X_F}} C_{l_r}$, per sec
L_β	$\frac{q_o Sb}{I_{X_F}} C_{l_\beta}$, per sec^2
N_p	$\frac{q_o Sb^2}{2VI_{Z_F}} C_{n_p}$, per sec
N_r	$\frac{q_o Sb^2}{2VI_{Z_F}} C_{n_r}$, per sec
N_β	$\frac{q_o Sb}{I_{Z_F}} C_{n_\beta}$, per sec^2
Y_β	$\frac{q_o S}{m_F V} C_{Y_\beta}$, per sec
Y_φ	$\frac{g}{V}$, per sec
L_δ	$\frac{q_o Sb}{I_{X_F}} C_{l_\delta}$, per sec^2
N_δ	$\frac{q_o Sb}{I_{Z_F}} C_{n_\delta}$, per sec^2
Y_δ	$\frac{q_o S}{m_F V} C_{Y_\delta}$, per sec
r_{X_F}	$\frac{I_{XZ}}{I_{X_F}}+\frac{q_o SbC_{l_{\ddot{\psi}}}}{I_{X_F}}$
r_{Z_F}	$\frac{I_{XZ}}{I_{Z_F}}$
L_p'	$L_p+r_{X_F}N_p$
L_β'	$L_\beta+r_{X_F}N_\beta$
N_r'	$N_r+r_{Z_F}L_r$
N_β'	$N_\beta+r_{Z_F}L_\beta$
L_δ'	$L_\delta+r_{X_F}N_\delta$
N_δ'	$N_\delta+r_{Z_F}L_\delta$

SUBSCRIPTS

B	body axis
DR	Dutch roll
cg	center of gravity
SP	short period
t	tail
wt	left wing tip

Dots are used to indicate differentiation with respect to time; for example, $\dot{\alpha}=\frac{d\alpha}{dt}$.

APPENDIX B

A METHOD FOR DETERMINING THE AERODYNAMIC LIFT AND MOMENT OF A FLEXIBLE WING THROUGH USE OF INFLUENCE COEFFICIENTS

The approach used is generally that presented in reference 11. However, for the calculation of wing deformations, the use of structural influence coefficients in conjunction with aerodynamic influence coefficients will be introduced in place of the wing bending and torsional stiffness distributions EI and GJ, and the distributed aerodynamic loadings used in reference 11.

LONGITUDINAL STABILITY DERIVATIVES

The loading on a flexible wing may be separated into two parts: that of the rigid wing and that produced by the wing deflection. The discussion that follows will be concerned with the determination of the loading produced by a wing deflection corresponding to a given rigid-wing loading. If a relaxation procedure is used in which successive deflections are calculated from each aerodynamic load (i. e., the first deflection due to the rigid wing aerodynamic loading, the second deflection due to the aerodynamic loading resulting from the first deflection and so on), then the change in streamwise angle of attack may be written as follows:

$$\epsilon(\eta)=\epsilon_0(\eta)q+\epsilon_1(\eta)q^2+\epsilon_2(\eta)q^3+\ \ldots \tag{B1}$$

where

$\epsilon_0(\eta)$ is the angle-of-attack distribution due to rigid-wing loading

$\epsilon_1(\eta)$ is the angle-of-attack distribution due to loading obtained from $\epsilon_0(\eta)$

$\epsilon_2(\eta)$ is the angle-of-attack distribution due to loading obtained from $\epsilon_1(\eta)$

The incremental angle-of-attack distributions $\epsilon_0(\eta)$, $\epsilon_1(\eta)$ may be converted into incremental lifts to form the series

$$\Delta C_L=C_{L_A}q+C_{L_B}q^2+C_{L_C}q^3+\ \ldots \tag{B2}$$

As noted in reference 11, this series can be represented by the equation

$$\Delta C_L=\frac{C_{L_A}q}{1+kq} \tag{B3}$$

if

$$k=-\frac{C_{L_B}}{C_{L_A}}=-\frac{C_{L_C}}{C_{L_B}},\ \text{etc.}^1$$

This result may be interpreted to mean that the successive wing-deflection shapes that produce these loads are essentially the same, and, hence, this portion of the wing loading may be represented as a single-degree-of-freedom system. Thus the incremental coefficient due to this portion of the wing deflections may be represented by the expression $C_{L_A}q/1+kq$ and it will be valid for large positive values of the quantity kq even though the series would not converge for positive kq greater than 1. The total lift coefficient for the flexible wing may then be written as

$$C_{L_F}=C_{L_R}\left(1+\frac{q}{1+kq}\frac{C_{L_A}}{C_{L_R}}\right) \tag{B4}$$

where C_{L_R} is the lift coefficient for the rigid wing. Similar equations may be written for the aerodynamic moment coefficient.

Thus it remains to determine C_{L_A}/C_{L_R} and k through use of the influence coefficients. The aerodynamic influence coefficients were obtained in the form of the loading coefficient $G_{\nu n}$ at a station ν due to a unit angle of attack at station n, the angle of attack at the other stations being zero. The loading coefficients were obtained by the method of reference 10. By use of this method, aerodynamic influence coefficients at four spanwise stations could be found which, with proper care, were sufficient to provide desired accuracy in determining wing deflections. These coefficients, $G_{\nu n}$, were obtained by assuming a unit angle of attack at one control point, and zero angle of attack at the remaining three, and then solving the set of four simultaneous equations consisting of the $a_{\nu n}$ coefficients obtained from reference 10. For instance, $G_{\nu 1}$ can be calculated from the following simultaneous equations

$$\begin{aligned}
1&=a_{11}G_{11}+a_{12}G_{21}+a_{13}G_{31}+a_{14}G_{41}\\
0&=a_{21}G_{11}+a_{22}G_{21}+a_{23}G_{31}+a_{24}G_{41}\\
0&=a_{31}G_{11}+a_{32}G_{21}+a_{33}G_{31}+a_{34}G_{41}\\
0&=a_{41}G_{11}+a_{42}G_{21}+a_{43}G_{31}+a_{44}G_{41}
\end{aligned}$$

where subscripts 1, 2, 3, and 4 refer to the semispan stations $\eta=0.924$, 0.707, 0.383, and 0. The resulting lift coefficient for each unit angle of attack can then be calculated using the equation

$$C_{L_n}=\frac{\pi A}{8}\left(G_{4n}+1.848G_{3n}+1.414G_{2n}+0.765G_{1n}\right) \tag{B5}$$

The experimentally determined structural influence coefficients (ref. 12) were measured in the form of deflections in inches at front and rear spars due to 1,000-pound loads at front and rear spars at a number of spanwise stations. These were cross-plotted to obtain the influence coefficients at the spanwise stations shown in table III. For use with the aerodynamic influence coefficients, these coefficients were further reduced into the form of a change in streamwise angle of attack in radians at station m, due to a 1,000-pound load at the quarter-chord position at station ν, $S_{m\nu}$.

[1] In reference 11, the constant k was determined by the ratios of the incremental deflections

$$k=-\frac{\epsilon_1(\eta)}{\epsilon_0(\eta)}=-\frac{\epsilon_2(\eta)}{\epsilon_1(\eta)},\ \text{etc.}$$

However, for the present method, it will be more convenient to deal directly with the incremental lifts.

The influence deflections due to a unit angle of attack at a control station can now be calculated through use of the aerodynamic and structural influence coefficients. In order to calculate the deflections with sufficient accuracy, an integration formula given in reference 10 was used.

$$\int_{-1}^{1} f(\eta)\, d\eta = \frac{\pi}{l+1} \sum_{\nu=1}^{l} f(\eta_\nu) \sin \phi_\nu$$

where $\phi_\nu = \frac{\nu\pi}{l+1}$ and $f(\eta_\nu)$ is the value of $f(\eta)$ at $\eta = \cos \frac{\nu\pi}{l+1}$. For the particular number of control stations used in the present case, and since $f(\eta_4)=0$, and using only the interval $0<\eta<1$, the integration formula becomes

$$\int_{0}^{1} f(\eta)\, d\eta = \sum_{\nu=1}^{3} f(\eta_\nu)\, I_\nu \tag{B6}$$

where

$$I_1 = 0.1502$$
$$I_2 = 0.2776$$
$$I_3 = 0.3628$$

Thus, the angular deflection at station m due to loading due to angle of attack at station n, with $q=1$ psi is calculated from the equation

$$(\epsilon_0)_{mn} = \frac{b^2(12)^2}{1000} \sum_{\nu=1}^{3} S_{m\nu} G_{\nu n} I_\nu \tag{B7}$$

with

$$m = 1, 2, 3$$
$$n = 1, 2, 3, 4$$

The resulting loading at station ν due to $(\epsilon_0)_{mn}$ is calculated from the equation

$$(G_A)_{\nu n} = \sum_{m=1}^{3} G_{\nu m} (\epsilon_0)_{mn} \tag{B8}$$

from which the lift coefficient may be obtained

$$(C_{L_A})_n = \frac{\pi A}{8} [(G_A)_{4n} + 1.848(G_A)_{3n} + 1.414(G_A)_{2n} + 0.765(G_A)_{1n}] \tag{B9}$$

The influence lift coefficient, $(C_{L_B})_n$, due to deflections due to the loading coefficient $(G_A)_{\nu n}$ can be calculated in a similar manner. The equation for $(C_{L_B})_n$ is

$$(C_{L_B})_n = \frac{\pi A}{8} [(G_B)_{4n} + 1.848(G_B)_{3n} + 1.414(G_B)_{2n} + 0.765(G_B)_{1n}] \tag{B10}$$

Thus, for a given angle-of-attack distribution, α_n, the lift resulting from the initial angle of attack and from the first and second twist distributions is calculated from the following equations

$$C_{L_R} = \sum_{n=1}^{4} C_{L_n} \alpha_n \tag{B11}$$

$$C_{L_A} = \sum_{n=1}^{4} (C_{L_A})_n\, \alpha_n \tag{B12}$$

$$C_{L_B} = \sum_{n=1}^{4} (C_{L_B})_n\, \alpha_n \tag{B13}$$

The total lift for the flexible wing may then be expressed as

$$C_{L_F} = C_{L_R} \left(1 + \frac{q \frac{C_{L_A}}{C_{L_R}}}{1+kq} \right) \tag{B14}$$

where

$$k = -\frac{C_{L_B}}{C_{L_A}}$$

A similar procedure is used to obtain the aerodynamic moment for a flexible wing.

Wing deflections may also be determined by means of wing-deflection influence coefficients in a manner similar to that which was used for determining the change in streamwise angle of attack. The deflection at station m due to the loading due to angle of attack at station n, with $q=1$ psi is calculated from the equation

$$(z_0)_{mn} = \frac{b^2(12)^2}{1000} \sum_{\nu=1}^{3} Z_{m\nu} G_{\nu n} I_\nu \tag{B15}$$

with

$$m = 1, 2, 3$$
$$n = 1, 2, 3, 4$$

where $Z_{m\nu}$ is the deflection in inches at station m due to a 1,000-pound load at the quarter chord at spanwise station ν.

For an arbitrary angle-of-attack distribution, the deflection at station m due to the initial load is

$$(z_0)_m = \sum_{n=1}^{4} (z_0)_{mn}\, \alpha_n \tag{B16}$$

The total deflection for the flexible wing may be developed in a manner similar to that used for equation (B14). Then

$$z_m = \frac{q}{1+kq} (z_0)_m \tag{B17}$$

in which the k from equation (B14) may be used with sufficient accuracy.

APPLICATION TO LATERAL-DIRECTIONAL STABILITY DERIVATIVES

In much the same manner as in the longitudinal derivatives, the rolling-moment coefficient resulting from an arbitrary antisymmetric angle-of-attack distribution may be expressed as a power series of the dynamic pressure q.

$$C_{l_F} = C_{l_R} + C_{l_A} q + C_{l_B} q^2 + C_{l_C} q^3 + \ldots \tag{B18}$$

where

C_{l_F} rolling-moment coefficient for the flexible wing

C_{l_R} rolling-moment coefficient for the rigid wing

$C_{l_A} q$ increment in rolling-moment coefficient resulting from structural deflections due to the C_{l_R} loading

$C_{l_B} q^2$ increment in rolling-moment coefficient resulting from structural deflections due to the C_{l_A} loading

For the wing structure considered in the present example, the ratios of all terms after the first one, $-C_{l_A}/C_{l_B}$, $-C_{l_B}/C_{l_C}$, etc., are essentially equal to a single constant k. The equation for rolling-moment coefficient for the flexible wing will then be

$$C_{l_F} = C_{l_R} \left[1 + \frac{q(C_{l_A}/C_{l_R})}{1+kq} \right] \tag{B19}$$

The quantities in equation (B19) will now be determined through use of aerodynamic and structural influence coefficients.

Antisymmetric aerodynamic influence coefficients were obtained through use of reference 18. First, $p_{\nu n}$ angle-of-attack influence coefficients, which represent the angle of attack at station ν due to a continuous loading function having a unit value at station n and zero value at the other stations, were obtained from reference 18. These were then converted to loading influence coefficients $A_{\nu n}$ (i. e., the loading $c_l c/2b$, at station, ν, due to a continuous angle-of-attack distribution with a unit value at station n and zero values at the other stations) by solving for the span loadings for a unit angle of attack at one control station. This was done for each of the spanwise control stations 1, 2, and 3 located at η=0.924, 0.707, and 0.383, respectively. The resulting rolling-moment coefficient for a unit angle of attack at a control station, n, can then be calculated using the following equation, which has the form of equation (15) in reference 18.

$$C_{l_n}=\frac{\pi A}{16}\left[A_{2n}+0.707(A_{1n}+A_{3n})\right] \tag{B20}$$

All aerodynamic loads were assumed to act along the quarter-chord line except for loads due to the ailerons. In an analogous manner to the symmetrical case, equation (B7), the change in streamwise angle of attack at station m due to the loading resulting from an angle of attack at station n, with q=1 psi, may be expressed as

$$(\epsilon_0)_{mn}=\frac{b^2(12)^2}{1000}\sum_{n=1}^{3} S_{m\nu}A_{\nu n}I_\nu \tag{B21}$$

with

$$m=1,\ 2,\ 3$$
$$n=1,\ 2,\ 3$$

where

$A_{\nu n}$ aerodynamic influence coefficients for the antisymmetric loading function at station ν due to an angle of attack at station n

The aerodynamic loading due to $(\epsilon_0)_{mn}$ is then obtained from the summation

$$(A_A)_{\nu n}=\sum_{m=1}^{3} A_{\nu m}(\epsilon_0)_{mn} \tag{B22}$$

from which the incremental rolling-moment coefficient may be obtained.

$$(C_{l_A})_n=\frac{\pi A}{16}\left\{(A_A)_{2n}+0.707\left[(A_A)_{1n}+(A_A)_{3n}\right]\right\} \tag{B23}$$

The next incremental rolling-moment coefficient $(C_{l_B})_n$ due to deflection resulting from the loading coefficients $(A_A)_{\nu n}$ is calculated in a similar manner.

Thus, the rolling-moment coefficients resulting from the initial angle of attack, and from the first and second twist distributions can be calculated from the following equations

$$C_{l_R}=\sum_{n=1}^{3} C_{l_n}\alpha_n \tag{B24}$$

$$C_{l_A}=\sum_{n=1}^{3} (C_{l_A})_n\alpha_n \tag{B25}$$

$$C_{l_B}=\sum_{n=1}^{3} (C_{l_B})_n\alpha_n \tag{B26}$$

The rolling-moment coefficient for the flexible wing for any desired angle-of-attack distribution, α_n, is then obtained by substituting values from the above equations into equation (B19). The reference rolling-moment coefficients with the aerodynamic loads at the quarter chord were calculated through use of the previous equations (with q=1 psi) and are tabulated in the following table:

n	1	2	3
C_{l_n}	0. 120	0. 298	0. 326
$C_{l_{A_n}}$	−. 0376	−. 0698	−. 0376
$C_{l_{B_n}}$	. 00856	. 01553	. 00796

In order to determine the rolling-moment coefficient for a specific derivative, the wing angle-of-attack distribution must be known. For a unit sideslip angle, the wing contribution to C_{l_β} may be separated into loadings due to two angle-of-attack distributions (ref. 19): (1) a constant spanwise angle-of-attack distribution due to the difference in effective velocity acting on each wing panel for the yawed attitude and (2) an angle-of-attack distribution proportional to the wing dihedral angle, which for this case may be considered to be due entirely to the upward deflection of the wings resulting from the level flight symmetrical air loads.

For the rigid airplane, the contribution to C_{l_β} due to the differential velocities acting on each wing panel was estimated from reference 20 as $C_{l_{\beta_1}}/C_L=-0.129$. Substituting values for a unit angle of attack into equations (B24), (B25), (B26), and (B19) gives

$$\frac{C_{l_{\beta_1}}}{C_L}=-0.129\left(1-\frac{\dfrac{0.1451}{0.744}q}{1+\dfrac{0.0321}{0.1451}q}\right)$$
$$=-0.129\left(1-\frac{0.195q}{1+0.221q}\right)$$

The dihedral angle, measured in a plane parallel with the YZ plane, was calculated through use of the influence coefficients for symmetrical loads and, for the flight range of interest, could be expressed as

$$\frac{\Gamma_{\eta=1}}{C_L}=0.1035q$$

The calculated distribution of dihedral angle, normalized with respect to the value at the tip, is given in the following table:

η	0. 383	0. 707	0. 924
Γ	. 520	. 900	. 992

For the wing at a unit angle of sideslip, these values of dihedral angle represent changes in the wing angle of attack, and the rolling-moment coefficient due to dihedral angle may be determined from equations given previously.

$$\frac{C_{l_{\beta_2}}}{C_L}=-(0.1035q)(0.557)\left(1-\frac{\frac{0.1197}{0.557}q}{1+\frac{0.02664}{0.1197}q}\right)$$

$$=-0.0577q\left(1-\frac{0.214q}{1+0.222q}\right)$$

Since only first-order effects have been considered, the changes in dihedral angle due to antisymmetric loads have been neglected.

The total value for the wing contribution to C_{l_β} becomes

$$\frac{C_{l_\beta}}{C_L}=\frac{C_{l_{\beta_1}}}{C_L}+\frac{C_{l_{\beta_2}}}{C_L}$$

$$\frac{C_{l_\beta}}{C_L}=-0.129\left(1-\frac{0.195q}{1+0.221q}\right)-0.0577q\left(1-\frac{0.214q}{1+0.222q}\right) \quad \text{(B27)}$$

While the two load distributions yield somewhat different values of the ratio C_{l_A}/C_{l_B}, the values of k are essentially the same. This was also found to be true for other types of load distributions. Note that the values of C_{l_β} obtained from equation (B27) are not the same as those given in table V since only the contribution of the wing has been considered here.

APPENDIX C

EVALUATION OF LONGITUDINAL STABILITY DERIVATIVES

C_{L_α}

Wing lift-curve slope.—This was determined theoretically from reference 10 and Appendix B using the section lift-curve slope of 5.71 as determined from wind-tunnel data supplied by the Boeing Airplane Company. This derivative should not be confused with the one in reference 21, which includes inertial effects. The present derivative is the one which would be evaluated experimentally in a wind tunnel with a flexible model.

Tail lift-curve slope.—This was determined in a manner similar to that of the wing, except that fuselage bending was included in the flexibility of the tail. It was found that the principal reduction in the tail lift-curve slope was caused by fuselage bending. Other factors included were the rate of change of downwash (ref. 22) and a tail efficiency factor of 0.95.

Body and nacelles lift-curve slope.—This was determined from wind-tunnel data supplied by the Boeing Airplane Company.

$C_{L_{\dot{\alpha}}}$

Lag in wing downwash.—Only the tail contribution was considered and was determined in a manner similar to that described in reference 23, including aeroelastic effects determined by the method of Appendix B. Although this term has small effect from the standpoint of lift, it is important in the calculation of $C_{m_{\dot{\alpha}}}$.

Normal acceleration.—Since normal acceleration is related to $\dot{\alpha}$ in the equation $n=-\frac{V}{g}(\dot{\theta}-\dot{\alpha})$, effects of structural deflections due to normal acceleration were included in derivatives in $\dot{\alpha}$ and $\dot{\theta}$ by the method of Appendix B. The principal contribution to this derivative is from the lift of the wing. Contribution of the tail varies according to the amount of fuel in the rear main tank and is from 10 to 20 percent of the total.

$C_{L_{\dot{\theta}}}$

Lift arising from angle-of-attack distribution due to pitching velocity (primarily a tail contribution) was determined using the method of Appendix B.

Normal acceleration.—Same as normal acceleration part of $C_{L_{\dot{\alpha}}}$, but of opposite sign.

$C_{L_{\ddot{\theta}}}$

Lift resulting from angle-of-attack distribution caused by structural distortion due to rotational inertial loads was determined by the method of Appendix B. This lift is contributed primarily by the wing but the total effect is small.

$C_{L_{\delta_e}}$

Rigid-airplane value was obtained from low-speed wind-tunnel data supplied by the Boeing Airplane Company and was assumed to be constant with Mach number. This is justified because the theoretical increase according to the Prandtl-Glauert rule is usually compensated by the pressure losses at the elevator hinge point (ref. 24). Aeroelastic effects of lift and moment on body bending and of lift on stabilizer distortion were included. Stabilizer distortion due to elevator pitching moment and elevator distortion were neglected.

C_{m_α}

The derivative was determined by multiplying the preceding C_{L_α} derivatives by the distance in mean aerodynamic chord lengths from their theoretical centers of pressure to the center of gravity. The value of C_{m_α} for body and nacelles was obtained by subtracting the theoretical C_{m_α} for wing alone from wind-tunnel values of C_{m_α} for wing, body, and nacelles. It should be noted that this also includes the change in C_{m_α} due to the difference between theoretical and experimental C_{m_α} of wing alone, a difference which is principally due to a somewhat higher loading near the root for the experimental than for the theoretical case. Since this additional loading occurs near the wing root, it does not affect the aeroelastic calculations and, hence, is appropriately added to C_{m_α} in the form of a correction for body pitching moment.

$C_{m_{\dot{\alpha}}}$, $C_{m_{\dot{\theta}}}$, $C_{m_{\ddot{\theta}}}$, $C_{m_{\delta_e}}$

These moment derivatives were determined by multiplying the corresponding lift derivatives by their moment arms in a manner similar to that described for C_{m_α}.

APPENDIX D

PREDICTED LATERAL-DIRECTIONAL AIRPLANE RESPONSE

EQUATIONS OF MOTION

The three lateral-directional equations of motion with respect to stability axes given in Appendix C of reference 3 for a rigid airplane will be modified for use for a flexible airplane. For the flexible case, additional terms must be added to take account of aerodynamic forces resulting from structural deflections due to inertial loads (C_{l_φ}, $C_{l_{\ddot{\psi}}}$, $C_{n_{\ddot{\psi}}}$, $C_{Y_{\dot{\psi}}}$, and $C_{Y_{\dot{\beta}}}$) and dead-weight loads (C_{Y_φ}). A more complete evaluation of these additional derivatives would also have included other derivatives dependent on $\ddot{\varphi}$, $\ddot{\psi}$, $\dot{\psi}+\dot{\beta}$, and φ. However, by the substitution of typical numerical values in the transfer-function coefficients, the cumulative effects of these other derivatives on the transfer-function coefficients were found to be negligible even though some of them were of appreciable size (e. g., ($C_{n_{\dot{\psi}}}$) and $C_{n_{\dot{\beta}}}$) were several times larger than $C_{n_r}(b/2V)$ for the largest values of M). The rolling moment, yawing moment, and side-force equations, with flight-path angle assumed zero, may be expressed as

$$\left(I_X D^2-q_o SbC_{l_{\ddot{\varphi}}}D^2-q_o SbC_{l_p}\frac{b}{2V}D\right)\varphi+\left(-I_{XZ}D^2-q_o SbC_{l_{\ddot{\psi}}}D^2-q_o SbC_{l_r}\frac{b}{2V}D\right)\psi-q_o SbC_{l_\beta}\beta=q_o SbC_{l_\delta}\delta \quad \text{(D1)}$$

$$\left(-I_{XZ}D^2-q_o SbC_{n_p}\frac{b}{2V}D\right)\varphi+\left(I_Z D^2-q_o SbC_{n_{\ddot{\psi}}}D^2-q_o SbC_{n_r}\frac{b}{2V}D\right)\psi-q_o SbC_{n_\beta}\beta=q_o SbC_{n_\delta}\delta \quad \text{(D2)}$$

$$(-W-q_o SC_{Y_\varphi})\varphi+(mVD-q_o SC_{Y_{\dot{\psi}}}D)\psi+(mVD-q_o SC_{Y_{\dot{\beta}}}D-q_o SC_{Y_\beta})\beta=q_o SC_{Y_\delta}\delta \quad \text{(D3)}$$

The remaining inertial deflection derivatives were then combined with the mass terms to form effective inertias for the flexible airplane. Thus

$$I_{X_F}=I_X-q_o SbC_{l_{\ddot{\varphi}}}$$

$$I_{Z_F}=I_Z-q_o SbC_{n_{\ddot{\psi}}}$$

$$m_F=m-\frac{q_o S}{V}C_{Y_{\dot{\beta}}}$$

$$\text{or } m-\frac{q_o S}{V}C_{Y_{\dot{\psi}}}$$

Since the derivatives $C_{Y_{\dot{\psi}}}$ and $C_{Y_{\dot{\beta}}}$ each represents aerodynamic forces due to lateral acceleration, they are of equal magnitude, and hence m_F may be expressed in terms of either derivative. The three equations (D1), (D2), and (D3) can then be written in a more convenient form by dividing them by I_{X_F}, I_{Z_F}, and $m_F V$, respectively, and introducing new symbols

$$(D^2-L_p D)\varphi+(-r_{X_F}D^2-L_r D)\psi-L_\beta\beta=L_\delta\delta \quad \text{(D4)}$$

$$(-r_{Z_F}D^2-N_p D)\varphi+(D^2-N_r D)\psi-N_\beta\beta=N_\delta\delta \quad \text{(D5)}$$

$$-Y_\delta\delta+D\psi+(D-Y_\beta)\beta=Y_\delta\delta \quad \text{(D6)}$$

Note that the term Y_φ (which equals g/V) remains the same as for the rigid case since the derivative C_{Y_φ} is due to dead-weight loads that are distributed in the same manner as the lateral acceleration loads.

TRANSFER FUNCTIONS

Transfer-function coefficients for φ/δ, ψ/δ, and β/δ can be obtained by simultaneous solution of the three equations (D4), (D5), and (D6).

Denominator coefficients.—The denominator of the transfer functions, Δ, may be expressed as

$$\Delta=D(C_4D^4+C_3D^3+C_2D^2+C_1D+C_0)$$

where

$$C_4=1-r_{X_F}r_{Z_F}$$

$$C_3=-L_p'-N_r'-Y_\beta(1-r_{X_F}r_{Z_F})$$

$$C_2=N_\beta'+Y_\beta(L_p'+N_r')+L_pN_r-N_pL_r$$

$$C_1=L_\beta N_p-N_\beta L_p-Y_\varphi L_\beta'+Y_\beta(L_rN_p-N_rL_p)$$

$$C_0=Y_\varphi(L_\beta N_r-N_\beta L_r)$$

For the moderate angle-of-attack range considered, r_{X_F} and r_{Z_F} are small quantities and hence $C_4\approx 1$. The denominator can then be expressed in factored form as

$$\Delta=\mathrm{D}(\mathrm{D}+\mathrm{D}_s)(D+D_r)(D^2+c_1D+c_2)$$

where D_s and D_r represent the spiral and rolling modes, respectively, and c_1 and c_2 are coefficients that define the damping and frequency of the Dutch roll mode.

Numerator coefficients.—With $p=D\varphi$, and $r=D\psi$, the numerator coefficients of the following transfer functions can be expressed in terms of the derivatives.

$$\frac{p}{\delta}=\frac{D(A_3D^3+A_2D^2+A_1D)}{\Delta}$$

where

$$A_3=L_\delta'$$

$$A_2=-Y_\beta L_\delta'+N_\delta L_r-L_\delta N_r+Y_\delta L_\beta'$$

$$A_1=L_\delta N_\beta-N_\delta L_\beta+Y_\beta(L_\delta N_r-N_\delta L_r)+Y_\delta(L_rN_\beta-N_rL_\beta)$$

$$\frac{r}{\delta}=\frac{D(B_3D^3+B_2D^2+B_1D+B_0)}{\Delta}$$

where

$$B_3=N_\delta'$$

$$B_2=L_\delta N_p-N_\delta L_p-Y_\beta N_\delta'+Y_\delta N_\beta'$$

$$B_1=Y_\beta(N_\delta L_p-L_\delta N_p)+Y_\delta(L_\beta N_p-N_\beta L_p)$$

$$B_0=Y_\varphi(L_\delta N_\beta-N_\delta L_\beta)$$

$$\frac{\beta}{\delta}=\frac{D(E_3D^3+E_2D^2+E_1D+E_0}{\Delta}$$

where

$$E_3=Y_\delta(1-r_{X_F}r_{Z_F})$$

$$E_2=-Y_\delta(N_r'+L_p')-N_\delta'$$

$$E_1=Y_\varphi L_\delta'+N_\delta L_p-L_\delta N_p+Y_\delta(L_pN_r-N_pL_r)$$

$$E_0=Y_\varphi(N_\delta L_r-L_\delta N_r)$$

Simplifications of the transfer functions.—When transfer functions are evaluated from measured data, it is desirable to use as simple a form as possible which will still adequately fit the data. Calculations indicated that the spiral mode factor D_s was very small and could be neglected for the frequency range of interest. Thus the rolling response to aileron was simplified to

$$\frac{p}{\delta_a}=\frac{A_3(D^2+a_1D+a_2)}{(D+D_r)(D^2+c_1D+c_2)}$$

where

$$a_1=\frac{A_2}{A_3}$$

$$a_2=\frac{A^1}{A_3}$$

To determine estimated values for use with the curve fitting of the measured responses on the analog computer, a partial fraction form of the transfer function was advantageous to use.

$$\frac{p}{\delta_a}=\frac{G_p}{D+D_r}+\frac{H_pD+J_p}{D^2+c_1D+c_2}$$

In obtaining approximate relations for $r\delta_r$ and β/δ_r, it was desirable first to write the transfer functions in partial fraction form.

$$\frac{r}{\delta_r}=\frac{F_r}{D+D_s}+\frac{G_r}{D+D_r}+\frac{H_rD+J_r}{D^2+c_1D+c_2}$$

$$\frac{\beta}{\delta_r}=\frac{F_\beta}{D+D_s}+\frac{G_\beta}{D+D_r}+\frac{H_\beta D+J_\beta}{D^2+c_1D+c_2}$$

By the substitution of typical numerical values, all numerator terms were found to be negligible except H_r and J_β. Thus, the transfer-function coefficients could be simplified to

$$\frac{r}{\delta_r}=\frac{H_rD}{D^2+c_1D+c_2}$$

$$\frac{\beta}{\delta}=\frac{J_\beta}{D^2+c_1D+c_2}$$

Transfer functions for the rear part of the fuselage and the wing tip.—In addition to the transfer-function coefficients for quantities at the center of gravity, the coefficients for r_t/δ, p_t/δ, and n_{wt}/δ are needed. The evaluation of these quantities includes responses at the center of gravity and also responses due to pseudostatic structural deflections at the particular location. The equation for yaw rate at the rear part of the fuselage is

$$\frac{r_t}{\delta}=\frac{r}{\delta}+\frac{D\Delta\psi_t}{\delta}$$

where $\Delta\psi_t$ represents the total change in angle of yaw in radians at the rear part of the fuselage due to structural deformations resulting from a control input. The following quantities were included in determining $\Delta\psi_t/\delta$

$$\frac{\Delta\psi_t}{\delta}=\frac{\Delta\psi_t}{\beta}\frac{\beta}{\delta}+\frac{\Delta\psi}{r}\frac{r}{\delta}+\frac{\Delta\psi_t}{\ddot{\psi}}\frac{\ddot{\psi}}{\delta}+\frac{\Delta\psi_t}{\delta}$$

For instance $\Delta\psi_t/\beta$ represents the pseudostatic change in angle of yaw at the rear part of the fuselage due to structural deformations resulting from a unit change in β.

Similarly, the equation for roll rate at the rear part of the fuselage is

$$\frac{p_t}{\delta}=\frac{p}{\delta}+\frac{D\Delta\varphi_t}{\delta}$$

where $\Delta\varphi_t$ represents the total change in angle of roll at the rear part of the fuselage due to structural deformations resulting from a control input and may be expressed as

$$\frac{\Delta\varphi_t}{\delta}=\frac{\Delta_{\varphi_t}}{\beta}\frac{\beta}{\delta}+\frac{\Delta_{\varphi_t}}{r}\frac{r}{\delta}+\frac{\Delta_{\varphi_t}}{\ddot{\psi}}\frac{\ddot{\psi}}{\delta}+\frac{\Delta_{\varphi_t}}{\delta}$$

The equation for acceleration at the left wing tip is

$$\frac{n_{wt}}{\delta}=-\frac{Dp}{\delta}+\frac{D^2z_{wt}}{12\delta}$$

Calculations indicated that the effect of D^2z_{wt}/δ was small for the frequency range up to the first antisymmetric bending frequency and, hence, was neglected.

Conversion of transfer-function coefficients from stability axes to body axes.—In order to compare predicted results with measured frequency responses which were obtained with respect to body axes, the predicted transfer functions were converted from stability-axis to body-axis form. Since, for the angle-of-attack range considered, the quantity C_4 was essentially unity, only the numerator terms of the transfer function need be modified. The equations for conversion from stability axes to body axes are (e. g., ref. 3).

$$p_B=p\cos\alpha-r\sin\alpha$$

$$r_B=r\cos\alpha+p\sin\alpha$$

$$\tan\beta_B=\frac{\tan\beta}{\cos\alpha}$$

For small angles of attack, the equations may be simplified to

$$p_B = p - r\alpha$$

$$r_B = r + p\alpha$$

$$\beta_B = \beta$$

These relations will also hold for derivatives of the angles. Hence, the numerator coefficients for p/δ and r/δ may be converted as follows:

$$A_{i_B} = A_i - B_i\alpha$$

$$B_{i_B} = B_i + A_i\alpha$$

REFERENCES

1. Seamans, R. C., Jr., Blasingame, B. P., and Clementson, G. C.: The Pulse Method for the Determination of Aircraft Dynamic Performance. Jour. Aero. Sci., vol. 17, no. 1, Jan. 1950, pp. 22–38.
2. Breaux, G. P., and Zeiller, E. L.: Dynamic Response Program on the B–36 Airplane. Part III—Presentation and Theoretical Considerations of the Transient Analysis Method Employed for Obtaining Frequency Response Functions from Flight Data. Rep. FZA–36–195, Consolidated Vultee Aircraft Corp., Feb. 14, 1952.
3. Triplett, William C., Brown, Stuart C., and Smith, G. Allan: The Dynamic-Response Characteristics of a 35- Swept-Wing Airplane as Determined From Flight Measurements. NACA Rep. 1250, 1955.
4. Marx, H. F., Clemen, A. T., and Zant, W. L.: Frequency Response Characteristics of the B–36D Airplane. Part I—Lateral Response at 40,000 Feet. Rep. FZA–36–256, Consolidated Vultee Aircraft Corp., Jan. 24, 1952.
5. Draper, Charles S., McKay, Walter, and Lees, Sidney: Instrument Engineering. Vol. 2. Methods for Associating Mathematical Solutions with Common Forms. McGraw-Hill Book Co., Inc., N. Y., 1953.
6. Cole, Henry A., Jr., and Bennion, Frances L.: Measurement of the Longitudinal Moment of Inertia of a Flexible Airplane. NACA TN 3870, 1956.
7. Schumacher, Lloyd E.: Methods for Analyzing Transient Flight Data to Obtain Aircraft Frequency Response. AF, Air Materiel Command, Wright-Patterson AFB (Flight Test Div. Memo Rep.) MCRFT–2268, 17 Jan. 1950.
8. Andrew, G. M.: End Correction for Flight-Tested Frequency Response Obtained by Laplace Transformation. Jour. Aero. Sci., vol. 19, no. 8, Aug. 1952, pp. 569–570.
9. Anon.: Flutter Inspection of Boeing XB–47 Airplane. AF, Air Materiel Command, Wright-Patterson AFB (Eng. Div. Memo Rep.) Ser. MCREXA5–4262–36–29, 9 Jan. 1948.
10. DeYoung, John, and Harper, Charles W.: Theoretical Symmetric Span Loading at Subsonic Speeds for Wings Having Arbitrary Plan Form. NACA Rep. 921, 1948.
11. Skoog, Richard B., and Brown, Harvey H.: A Method for the Determination of the Spanwise Load Distribution of a Flexible Swept Wing at Subsonic Speeds. NACA TN 2222, 1951. (Supersedes NACA RM A50G31).
12. Mayo, Alton P., and Ward, John F.: Experimental Influence Coefficients for the Deflection of the Wing of a Full-Scale, Swept-Wing Bomber. NACA RM L53L23, 1954.
13. Shinbrot, Marvin: A Least Squares Curve Fitting Method With Applications to the Calculation of Stability Coefficients From Transient-Response Data. NACA TN 2341, 1951.
14. Brown, R. B., and Perkins, Grace: Full Scale Test of the XB–47 Empennage. Part II—Pressure Data. Boeing Airplane Co. Document No. D–8517–1, Oct. 27, 1948.
15. White, Roland J.: Investigation of Lateral Dynamic Stability in the XB–47 Airplane. Jour. Aero. Sci., vol. 17, no. 3, Mar. 1950, pp. 133–148.
16. Swenson, Floyd: Fin and Rudder Destruction Tests, Model B–47B. Boeing Airplane Co., Test No. 25308, Apr. 18, 1951.
17. Cole, Henry A., Jr., Brown, Stuart C., and Holleman, Euclid C.: The Effects of Flexibility on the Longitudinal and Lateral-Directional Response of a Large Airplane. NACA RM A55D14, 1955.
18. DeYoung, John: Theoretical Antisymmetric Span Loading for Wings of Arbitrary Plan Form at Subsonic Speeds. NACA Rep. 1056, 1951. (Formerly NACA TN 2140).
19. Miles, John W.: The Rolling Moment Due to Sideslip for a Swept Wing. Jour. Aero. Sci., vol. 15, no. 7, July 1948, pp. 418–424.
20. Holtby, K., and Seiler, R.: Development of Lateral Controls for Flexible Swept Wings. Boeing Airplane Co. Document No. D–9458, Apr. 6, 1950.
21. Skoog, Richard B.: An Analysis of the Effects of Aeroelasticity on Static Longitudinal Stability and Control of a Swept-Wing Airplane. NACA Rep. 1298, 1957. (Supersedes NACA RM A51C19).
22. Diederich, Franklin W.: Charts and Tables for Use in Calculations of Downwash of Wings of Arbitrary Plan Form. NACA TN 2353, 1951.
23. Perkins, Courtland D., and Hage, Robert E.: Airplane Performance Stability and Control. John Wiley & Sons, Inc., 1949.
24. Tinling, Bruce E., and Dickson, Jerald K.: Tests of a Model Horizontal Tail of Aspect Ratio 4.5 in the Ames 12-Foot Pressure Wind Tunnel. I—Quarter-Chord Line Swept Back 35°. NACA RM A9G13, 1949.

U. S. GOVERNMENT PRINTING OFFICE: 1958